Final Project Report

Project Title: Efficient Discovery of Novel Multicomponent Mixtures for Hydrogen Storage: A Combined Computational/Experimental Approach

Project Dates: Sept. 2008 – Aug. 2014
Date of Report: Nov. 28, 2016

Recipient: Northwestern University
Award Number: DE-FG36-08GO18136

Working Partners:
PI: Prof. Christopher Wolverton
Department of Materials Science & Engineering
Northwestern University
Evanston, IL 60208
E-mail: c-wolverton@northwestern.edu
Phone: 847-467-0593
Fax: 847-491-7820

Co-PI: Prof. Vidvuds Ozolins
Department of Materials Science & Engineering
University of California, Los Angeles
Los Angeles, CA 90505-1959
E-mail: vidvuds@ucla.edu
Phone: (310) 267-5538
Fax: (310) 206-7353

Co-PI: Prof. Harold H. Kung
Department of Chemical and Biological Engineering
Northwestern University
Evanston, IL 60208
E-mail: hkung@northwestern.edu
Phone: (847) 491-7492
Fax: (847) 467-1018

Cost-Sharing Partners:
Co-PIs: Dr. Jun Yang
Ford Motor Company
Ford Research and Innovation Center
MD 3028/RIC
Dearborn, MI 48121
E-mail: jyang27@ford.com
Phone: (313) 390-1376
Fax: (313) 594-2963

Co-PIs: Dr. Sonjong Hwang
Chemistry and Chemical Engineering
California Institute of Technology
Pasadena, CA 91125
E-mail: sonjong@cheme.caltech.edu
Phone: (626)395-2323
Fax: (626)568-8743

Co-PIs: Prof. Sheldon Shore
Department of Chemistry and Biochemistry
The Ohio State University
Columbus, OH 43210
E-mail: shore@chemistry.ohio-state.edu
Phone: (614)292-6000
Fax: (614)292-1685

Contact:
PI: Prof. Christopher Wolverton
Department of Materials Science & Engineering
Northwestern University
Evanston, IL 60208
E-mail: c-wolverton@northwestern.edu
Phone: 847-467-0593
Fax: 847-491-7820

DOE Managers: Katie Randolph

Project Objective:
The objective of the proposed program is to discover novel mixed hydrides for hydrogen storage, which enable the DOE 2010 system-level goals. Our goal is to find a *material* that desorbs 8.5 wt.% H_2 or more at temperatures below 85 ^oC. The research program will combine first-principles calculations of reaction thermodynamics and kinetics with material and catalyst synthesis, testing, and characterization. We will combine materials from distinct categories (e.g., chemical and complex hydrides) to form novel multicomponent reactions. Systems to be studied include mixtures of complex hydrides and chemical hydrides [e.g. $LiNH_2$+NH_3BH_3] and nitrogen-hydrogen based borohydrides [e.g. $Al(BH_4)_3(NH_3)_3$].

Background:
The 2010 and 2015 FreedomCAR/DOE targets for hydrogen storage systems are very challenging, and cannot be met with existing materials. The vast majority of the work to date has delineated materials into various classes, e.g., complex and metal hydrides, chemical hydrides, and sorbents. However, very recent studies indicate that *mixtures* of storage materials, particularly mixtures *between various classes*, hold promise to achieve technological attributes that materials within an individual class cannot reach.

Our project involves a systematic, rational approach to designing novel multicomponent mixtures of materials with fast hydrogenation/dehydrogenation kinetics and favorable thermodynamics using a combination of state-of-the-art scientific computing and experimentation. We will use the accurate predictive power of first-principles modeling to understand the thermodynamic and microscopic kinetic processes involved in hydrogen release and uptake and to design new material/catalyst systems with improved properties. Detailed characterization and atomic-scale catalysis experiments will elucidate the effect of dopants and nanoscale catalysts in achieving fast kinetics and reversibility. And, state-of-the-art storage experiments will give key storage attributes of the investigated reactions, validate computational predictions, and help guide and improve computational methods. In sum, our approach involves a powerful blend of: 1) H2 Storage measurements and characterization, 2) State-of-the-art computational modeling, 3) Detailed catalysis experiments, 4) In-depth automotive perspective.

Results:

We begin with a brief discussion of many of the published results, along with citation information. We follow that with some of the more significant findings of the project that have not been published. Please note that in each section, the figures and references are numbered separately for each section (i.e., figures/references start at "1" in each section).

I. Theoretical prediction of different decomposition paths for $Ca(BH_4)_2$ and $Mg(BH_4)_2$

Yongsheng Zhang, Eric Majzoub, Vidvuds Ozolins and C. Wolverton
Phys. Rev. B **82**, 174107 (2010)

We have studied the decomposition pathways of both Ca- and Mg-borohydride using density-functional theory (DFT) calculations of the free energy (including vibrational contributions) in conjunction with a Monte Carlo-based crystal-structure prediction method, the prototype electrostatic ground-state (PEGS) search method. We find that a recently proposed CaB2H2 intermediate (M. D. Riktor, M. H. Sørby, K. Chłopek, M. Fichtner, and B. C. Hauback, J. Mater. Chem. **19**, 2754 (2009)] is energetically highly unfavorable and hence very unlikely to form. We systematically search for low-energy structures of CaB2H*n* compounds with *n*=2, 4, and 6 using PEGS simulations, refining the resulting structures with accurate DFT calculations. We find that the lowest-energy CaB2H2 and CaB2H4 crystal structures do not lie on the thermodynamically stable decomposition path but rather are unstable with respect to a decomposition pathway involving the previously proposed CaB12H12 phase. We also predict a CaB2H6 compound which forms a low-energy intermediate in the calcium borohydride decomposition pathway. This new reaction pathway is practically degenerate with decomposition into the CaB12H12 phase. Similar calculations for magnesium borohydride show that a recently predicted MgB2H6 phase does not form a stable intermediate in the decomposition pathway of Mg(BH4)2.

II. Prediction of a $Ca(BH_4)(NH_2)$ quaternary hydrogen storage compound from first-principles calculations
Dilpuneet S. Aidhy, Yongsheng Zhang and C. Wolverton
Phys. Rev. B **84**, 134103 (2011)

We use a combination of density functional theory (DFT) calculations and a Monte Carlo (MC)-based crystal structure prediction tool, the Prototype Electrostatic Ground State (PEGS) method, to search for new hydrogen storage compounds in the Ca-based mixed–amide-borohydride quaternary system. We predict the existence of a new ordered quaternary compound, CaBNH6, whose stoichiometry comes from a 1:1 mixture of Ca(BH4)2 and Ca(NH2)2. Our DFT calculations show that CaBNH6 is !12.5 kJ/mol Ca (at T = 0 K) lower in energy than the mixture of 1/2[Ca(BH4)2 + Ca(NH2)2]. DFT phonon calculations of vibrational thermodynamics show that this stability of CaBNH6 [with respect to Ca(BH4)2 and Ca(NH2)2] persists to finite temperatures. The predicted crystal structure contains two formula units of CaBNH6. We have also performed a thermodynamic analysis of hydrogen decomposition of our predicted compound using the Grand Canonical Linear Programming (GCLP) method combined with a large database of DFT energies and vibrational thermodynamics. We find that the thermodynamically preferred decomposition reaction for CaBNH6 involves formation of BN with a low decomposition enthalpy. Though the decomposition enthalpy is low, the kinetic behavior of CaBNH6 decomposition is not yet known. We assert that further experimental investigation of this system is warranted to verify the existence of predicted quaternary compounds in this Ca-B-N-H system, as well as to elucidate their hydrogen release reaction pathways.

III. First-principles prediction of high-capacity, thermodynamically reversible hydrogen storage reactions based on (NH4)2B12H12
W. H. Sun, C. Wolverton, A. R. Akbarzadeh and V. Ozolins
Phys. Rev. B 83, 064112 (2011)

We use a combination of first-principles density functional calculations along with the recently developed grand canonical linear programing method to predict a novel, high capacity hydrogen storage reaction with thermodynamics suitable for near-ambient reversible storage. Unlike the vast majority of previously proposed complex hydrides, which typically rely on a hydrogen-containing *anionic* unit, our reaction is based on an ammonium-containing hydride, (NH4)2B12H12, which contains increased storage capacity due to *both anionic and cationic* hydrogen-containing complexes. The predicted decomposition of this hydride is a two-step reaction sequence: (NH4)2B12H12 → 2BN + 1/2B20H16 + 6H2 →2BN + 10B + 10H2, which possesses a theoretical gravimetric capacity of 11.3 wt% H2, a single-crystal volumetric density of 104 g H2/L, and T = 300 K reaction enthalpies of 17 and 33 kJ/mol H2, respectively, which are well-suited for near-ambient reversible storage. The combination of these

three attributes in a single material makes this decomposition reaction sequence highly promising.

IV. Theoretical prediction of metastable intermediates in the decomposition of $Mg(BH_4)_2$

Yongsheng Zhang, Eric Majzoub, Vidvuds Ozolins and C. Wolverton
J. Phys. Chem. C **116**, 10522 (2012)

We have studied the decomposition pathway and products of Mg-borohydride using density functional theory (DFT) calculations of free energy (including vibrational contributions) in conjunction with a Monte Carlo-based crystal structure prediction method, the prototype electrostatic ground state (PEGS) search method. We find that a recently proposed Mg(B3H8)2 intermediate (Chong et al. Chem. Commun. 2011, 47, 1330) is energetically highly unfavorable with respect to decomposition into MgB12H12 and hence is not a thermodynamic reaction product. We systematically search for low-energy structures of Mg-triboranes [Mg-(B3H8)2, MgB3H7, and Mg3(B3H6)2], closo-borane MgBnHn (n = 6, 7, 8, 9, 10, 11), and Mg(B11H14)2 compounds using PEGS simulations, refining the resulting structures with accurate DFT calculations. We find that none of these compounds break the previously determined thermodynamically stable decomposition path: Mg(BH4)2 → 1/6MgB12H12 + 5/6MgH2 + 13/6H2 → MgB2 + 4H2. However, the reaction [Mg(BH4)2 → 1/3Mg3(B3H6)2 + 2H2] involving a Mg3(B3H6)2 product has an enthalpy close to that of the MgB12H12 pathway and falls within the desired enthalpy window for near-ambient reversibility [20−50 kJ/ (mol H2)]. This indicates that (1) if MgB12H12 is kinetically hindered in the decomposition of Mg(BH4)2 such as in the aforementioned reference (Chong et al. Chem. Commun. 2011, 47, 1330), Mg3(B3H6)2 might be yielded as a metastable intermediate, and (2) Mg3(B3H6)2 could possibly be rehydrided back to Mg(BH4)2 under modest H2(T,p) conditions. We suggest that the observed intermediate is not [B3H8] but could be another triborane such as [B3H6].

V. Crystal structures, phase stabilities, and hydrogen storage properties of metal amidoboranes

Yongsheng Zhang and C. Wolverton
J. Phys. Chem. C **116**, 14224 (2012)

Metal amidoboranes, M(NH2BH3)n (M = alkali metal or alkaline-earth metal), are candidates for on-board hydrogen storage materials with high gravimetric capacity, low H2 release temperature, and the ability to suppress toxic borazine emission. We have used a first principles density functional theory (DFT) combination with Monte Carlo method to search for crystal structures for a wide array of metal amidoboranes (M = Li, Na, K, Be, Mg, Ca, Sr, and Sc). In cases where the experimental structures are known, the DFT energies of the theoretically predicted LiNH2BH3, NaNH2BH3, KNH2BH3, and Ca(NH2BH3)2 structures are degenerate with the DFT energies computed for the experimental structures [to within 4 kJ/(mol f.u.)], confirming the accuracy of our

approach. On the basis of the decomposition reaction pathway, M(NH2BH3)n → MHn + nBN + 2nH2, we compute the H2 release reaction enthalpies and show that the stability of metal amidoboranes obeys the following trend: The metal amidoborane becomes more stable (the decomposition reaction becomes less exothermic) as the metal cation becomes more electropositive, that is, as the metal cation goes down in the periodic table along a given column or as the metal moves to the left along a given row. The only exception to this rule is Mg(NH2BH3)2, which is more stable than Ca(NH2BH3)2. Introducing vibrational entropy effects does not change this exceptional behavior of Mg amidoborane: the phonon contribution serves to shift all reaction enthalpies down by a roughly constant amount, ∼22 kJ/ (mol H2) at T = 300 K

VI. First principles studies of phase stability and crystal structures in Li-Zn mixed-metal borohydrides
Yongli Wang, Yongsheng Zhang and C. Wolverton
Phys. Rev. B **88**, 024119 (2013)

We address the problem of finding mixed-metal borohydrides with favorable thermodynamics and illustrate the approach using the example of LiZn2(BH4)5. Using density functional theory (DFT), along with the grandcanonical linear programming method (GCLP), we examine the experimentally and computationally proposed crystal structures and the finite-temperature thermodynamics of dehydrogenation for the quaternary hydride LiZn2(BH4)5.We find the following: (i) For LiZn2(BH4)5, DFT calculations of the experimental crystal structures reveal that the structure from the neutron diffraction experiments of Ravnsbæk *et al.* is more stable [by 24 kJ/(mol f.u.)] than that based on a previous x-ray study. (ii) Our DFT calculations show that when using the neutron diffraction structure of LiZn2(BH4)5, the recently theoretically predicted LiZn(BH4)3 compound is unstable with respect to the decomposition into LiZn2(BH4)5 + LiBH4. (iii) GCLP calculations show that even though LiZn2(BH4)5 is a combination of weakly [Zn(BH4)2] and strongly (LiBH4) bound borohydrides, its decomposition is not intermediate between the two individual borohydrides. Rather, we find that the decomposition of LiZn2(BH4)5 is divided into a weakly exothermic step [LiZn2(BH4)5 → 2Zn + 1/5LiBH4 + 2/5 Li2B12H12 + 36/5 H2] and three strong endothermic steps (12LiBH4 → 10LiH + Li2B12H12 + 13H2; Zn+ LiH → LiZn + 1/2H2; 2Zn + Li2B12H12 → 2LiZn + 12B + 6H2). DFT-calculated enthalpy values for the first three LiZn2(BH4)5 decomposition steps are −19, +37, +74 kJ/(mol H2), respectively. The behavior of LiZn2(BH4)5 shows that mixed-metal borohydrides formed by mixing borohydrides of high and low thermodynamics stabilities do not necessarily have an intermediate decomposition tendency. ***Our results suggest the correct strategy to find intermediate decomposition in mixed-metal borohydrides is to search for stable mixed metal products such as ternary metal borides.***

VII. Crystal structure, phase stability, and decomposition of the quaternary Mg-B-N-H hydrogen storage system
Yongsheng Zhang, David Farrell, Jun Yang, Andrea Sudik and C. Wolverton,
J. Phys. Chem. C 118, 11193 (2014).

Using the combination of DFT-based computational approaches and experimental measurements, we have studied the crystal structure, phase stability, and decomposition products of mixed Mg(NH2)2/Mg(BH4)2 materials. We find the following: (i) DFT crystal structure prediction calculations (0 K) show the existence of a mixed Mg(NH2)2/Mg(BH4)2 phase, which is thermodynamically stable relative to its separated phases [Mg(NH2)2 and Mg(BH4)2]. (ii) The DFT calculated phonon density of states of Mg(NH2)(BH4) is in good agreement with the peak positions from experimental PAS IR measurements (at the room temperature) of a ball-milled Mg(NH2)2/Mg(BH4)2 mixture, suggesting the mixture is not merely a physical mixture of the individual compounds. (iii) The experimentally measured dehydrogenation temperature of the mixed Mg(NH2)2/Mg(BH4)2 phase is lower than that of Mg(NH2)2 or Mg(BH4)2, which further confirms that it is not a simply physical mixture of Mg(NH2)2 and Mg(BH4)2. The observed amount of H2 release is 3.4 wt % at 250° and 8.3 wt % above 280°. (iv) From a combination of DFT, the grand-canonical linear programming (GCLP) method calculations, and PAS IR measurements of dehydrogenated samples, we identify the existence of the B−H bonds and linear N−B−N units in the decomposition of Mg(NH2)2/Mg(BH4)2. (v) Experimental desorption measurements reveal that the Mg(NH2)2/Mg(BH4)2 mixed phase is irreversible, consistent with DFT calculated enthalpies in the range of −18 to +16 kJ/(mol H2), too low for near ambient reversible storage.

VIII. Thermodynamic stability of transition metals on the Mg-terminated MgB2 (0001) surface and their effects on hydrogen dissociation and diffusion
Yongli Wang, Kyle Michel, Yongsheng Zhang and C. Wolverton, Phys. Rev. B 91, 155431 (2015).

The hydrogenation of MgB2 is a critical step in the reversibility of several well-known hydrogen storage reactions. Of the many processes that must occur during rehydrogenation, at least two of them take place near the surface: the dissociation of H2 molecules and the subsequent diffusion of atomic hydrogen. Using first-principles calculations, we determine the energetic barriers for these processes on the ideal Mg terminated MgB2 (0001) surface, as well as on surfaces containing transition metal dopants (Sc-Zn, Y-Cd, Pt, and Au). The calculated dissociation barrier for H2 on the clean surface is 0.89 eV, and the surface diffusion barrier is 0.17 eV. However, we find examples of dopants that significantly decrease the activation barrier for the dissociation of H2. Our calculations suggest that Ni, Cu, and Pd are good catalytic candidates for the surface processes involved in MgB2 rehydrogenation.

IX. Hydrogen diffusion in MgB_2 bulk
Y.L. Wang, K. Michel, and C. Wolverton, Scripta Materialia **117**, 86 (2016).

The diffusion of hydrogen inMgB2 is crucial to the kinetics of rehydrogenation of Mg(BH4)2.We report a comprehensive combination of first-principles calculations and

Kinetic Monte Carlo Simulations to examine the energetics of diffusion of hydrogen atoms through bulk MgB2. From these calculations we find that diffusion is fast for the neutral interstitial hydrogen defect and that the overall migration barrier for hydrogen diffusion in MgB2 is 0.22 eV, showing that rapid diffusion of hydrogen is possible even at moderate temperatures. The interstitial hydrogen defect formation energy is around 0.8 eV at 0 K, indicating a low hydrogen solubility at moderate temperatures.

X. First-principles insight into the degeneracy of ground state $LiBH_4$ structures
Yongsheng Zhang, Yongli Wang, Kyle Michel and C. Wolverton
Phys. Rev. B **86**, 094111 (2012)

Recently, a number of ground-state structures of LiBH4 have been proposed, both from experimental and computational works. The results showcontroversy between computational and experimental ground-state crystal structures of LiBH4. In order to determine which is truly the lowest in energy, we study LiBH4 in a variety of crystal structures using density functional theory (DFT) calculations of the free energy (T = 0 K total energy plus vibrational thermodynamics), employing a variety of DFT methods and exchange-correlation functionals. Our calculations show that the experimentally observed structures are lowest in energy in DFT. However, multiple LiBH4 structures are degenerate with the experimental ground-state crystal structure and there exists a relatively flat potential energy landscape between them. These degenerate structures include the recently theoretically predicted LiBH4 structure [Tekin, Caputo, and Z¨uettel, Phys. Rev. Lett. **104**, 215501 (2010)], which the authors claimed to be 9.66 kJ/(mol LiBH4) (or ∼100 meV/fu) lower in energy than the experimentally XRD determined LiBH4 structure [Soulie´, Renaudin, C˘ erny´, and Yvon, J. Alloys Compd. **346**, 200 (2002)]. Our calculations do not support these previous claims, and hence resolve this discrepancy between DFT and experiment.

XI. Structure determination of an amorphous compound AlB_4H_{11}
Xuenian Chen, Yongsheng Zhang, Yongli Wang, Wei Zhou, Douglas A. Knight, Teshome B. Yisgedu, Zhenguo Huang, Hima K. Lingam, Beau Billet, Terrence J. Udovic, Terrence J. Udovic, Gibert M. Brown, Sheldon G. Shore, Christopher M. Wolverton and Ji-Cheng Zhao
Chem. Sci. **3**, 3183 (2012)

The structure of the amorphous aluminoborane compound AlB4H11 was identified through a collaborative study closely coupling a first-principles density functional based approach with experimental measurements using IR, NMR, and neutron vibrational spectroscopy (NVS). The AlB4H11 structure was found to contain distinct [BH4] and [B3H7] units without any [AlH4] units. It forms a –[B3H7]–Al(BH4)– polymer chain with the [BH4] units twisted relative to each other perpendicular to the chain direction and bonded to Al, and a chain backbone consists of [B3H7] and Al where the [B3H7] unit exhibits a triangular boron configuration. The computed lowest energy structure shows good agreement with results of IR, NVS and NMR spectra; this agreement

demonstrates the extended applicability of the structure prediction approach to the prediction of even amorphous compounds.

XII. First-principles prediction of intermediate products in the decomposition of metal amidoboranes

Yongsheng Zhang, Tom Autrey and C. Wolverton
J. Phys. Chem. C **116**, 26728 (2012)

The nonvolatile products remaining after the thermal decomposition of metal amidoboranes (MAB, M = metal) are amorphous and incompletely characterized, increasing the complexity of devising regeneration strategies for these potential hydrogen storage materials. Utilizing the combined prototype electrostatic ground state search and density-functional theory (PEGS+DFT), we find that potential reaction products ($[NHBH_2]^-$, $[NBH]^-$, $[N_3H_2B_3H_3]^-$, and polymer-$M[NHBH_2]$ anion groups) in the decomposition of LiAB and CaAB are calculated to be significantly endothermic, in contrast to the experimentally measured nearly thermoneutral values [~ -4 kJ/(mol H_2) in LiAB and 3.5 kJ/(mol H_2) in CaAB], suggesting that there are alternative products formed. The dianion group $[NHBHNHBH_3]^{2-}$ has recently been suggested to form in the decomposition of a calcium amidoborane complex in solution. In LiAB and CaAB, we use PEGS+DFT to predict intermediate metal–dianion compounds, and the static H_2 release enthalpy is 27.4 and 27.3 kJ/(mol H_2) in LiAB and CaAB, respectively. Introducing vibrational effects by phonon calculations, the enthalpies are shifted down by a roughly constant amount, $\sim$25 and $\sim$22 kJ/(mol H_2) at 0 and 300 K. Thus, our theoretical H_2 release enthalpies agree with the experimentally measured nearly thermoneutral data in the decomposition of LiAB and CaAB. This agreement supports the existence of the dianion phases as products in the decomposition of metal amidoboranes. Then, using the dianion compound as an intermediate in the decomposition of MAB, we further study the stability trends of a series of MAB (M = Li, Na, K, Ca).

XIII. Fast Mass Transport Kinetics in $B_{20}H_{16}$: A High-Capacity Hydrogen Storage Material

Kyle Michel, Yongsheng Zhang and C. Wolverton
J. Phys. Chem. C **117**, 19295 (2013)

The storage of hydrogen in an economical and practical way remains a significant challenge in the development of hydrogen fuel cell vehicles. Reversible storage in the solid state (such as in complex metal hydrides) has gained much interest due to the favorable storage densities that can be achieved. A candidate material must release hydrogen at a few bar and operate using the waste heat from the PEM fuel cell. Well-established methods such as the Grand Canonical Linear Programming method (GCLP) have been used to screen hydrogen storage reactions using energetics obtained from first-principles calculations in order to determine those that are thermodynamically allowable. Besides releasing and absorbing hydrogen in the target range of temperatures and pressures, these reactions should occur rapidly where the targeted rehydrogenation rate proposed by the Department of Energy (DOE) is 2.0 kg H_2/min. Of the known hydrogen storage reactions that have thermodynamic properties and storage capacities that meet the DOE targets, all suffer from unacceptably slow reaction rates.

There are many processes that may limit the dehydrogenation or rehydrogenation rates of metal hydrides such as nucleation, growth, and H_2 dissociation and recombination at surfaces. In particular, many studies have focused on the kinetics of long-range mass transport during the growth stage. There is both experimental and theoretical evidence that this mass transport step occurs via the diffusion of point defects through bulk phases and that it may be rate limiting in many reactions. This provides motivation to determine the mass transport barrier for proposed reactions. Those reactions with high mass transport barriers can be disregarded for practical applications since their kinetics will be unacceptably slow, unless a suitable catalyst can be found.

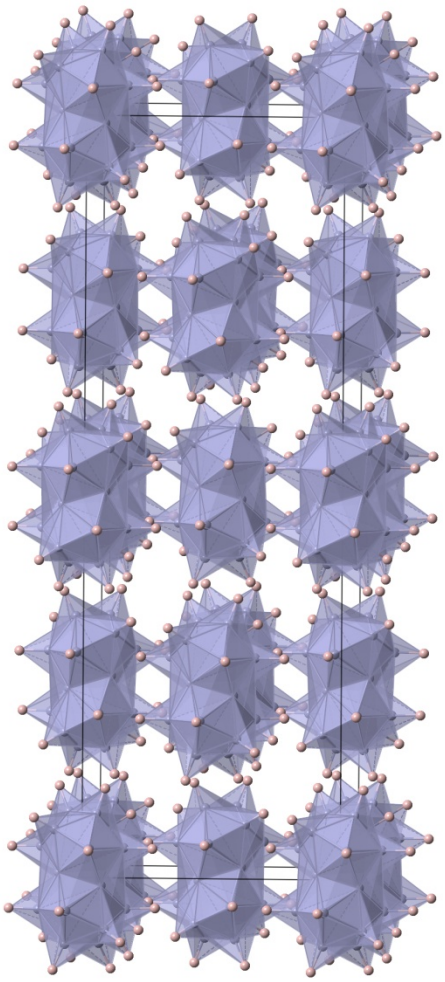

Fig. 1 Structure of $B_{20}H_{16}$ with B atoms represented by purple spheres, H atoms by pink spheres , and $B_{20}H_{16}$ clusters by polyhedra.

Recently, the decomposition of $B_{20}H_{16}$(Fig. 1) has been predicted to occur via a single-step reaction:
$B_{20}H_{16} \rightarrow 20B + 8H_2$

The enthalpy change of Reaction is equal to 33 kJ/mol H_2 with a calculated equilibrium temperature of 20 °C (at a pressure of 1 bar H_2), releasing 6.9 wt. % H_2 with a volumetric density of 64.1 g H_2/L. These thermodynamic properties and large storage capacity makes this reaction attractive for applications in passenger vehicles. We focus on the kinetics of mass transport in Reaction.

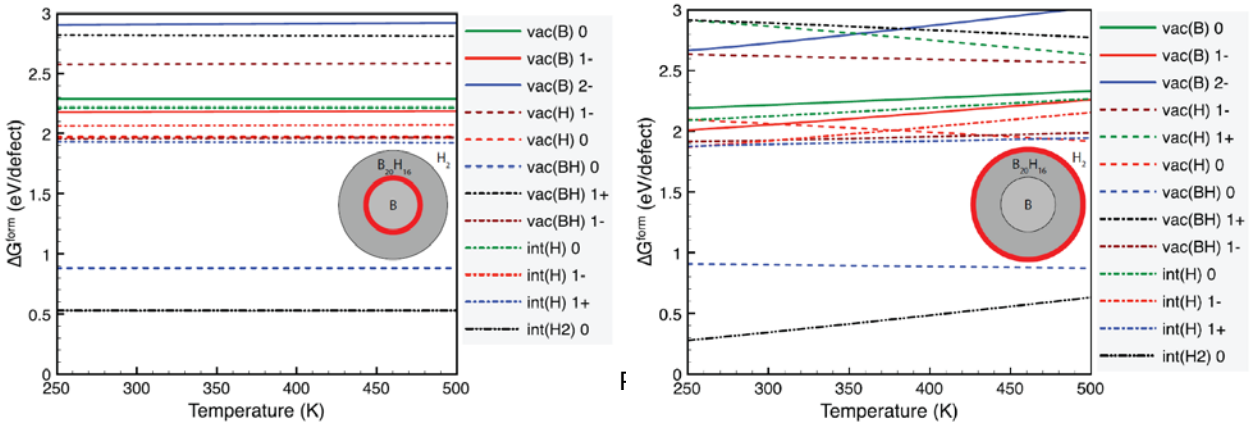

Fig2. Free energies of formation for defects in B20H16. Only those defects with formation energies of less than 3 eV are shown. The bold red lines on the inset morphologies show the interfaces at which each set of formation energies is calculated.

Free energies of formation for defects are plotted versus temperature in Fig. 2 at both of the interfaces inserted in Fig. 2. Of the defects in $B_{20}H_{16}$, we find that interstitial H_2 has the lowest free energy of formation under all assumed conditions; it is equal to 0.55 eV/defect at the $B/B_{20}H_{16}$ interface and increases from 0.28 to 0.63 eV/defect at the $B_{20}H_{16}/H_2$ interface as the temperature is increased from 250 to 500 K. This temperature dependence of the free energy of formation is due to the chemical potential of hydrogen gas, which decreases with increasing temperature. Of the remaining defects, the formation energy of neutral BH vacancies is several hundred meV above that of interstitial H_2 and all other defect formation energies are still higher by at least 1 eV. From steric arguments used in most crystals, it is somewhat surprising that an H_2 dimer, instead of some other monatomic type, is the lowest-energy interstitial defect. However, since $B_{20}H_{16}$ is a molecular crystal, there exist large voids in the structure in which it is possible that both atoms in an H_2 dimer can each be more than 1.5 Å from any other atom in the crystal. This large distance between the H_2 dimer and the host $B_{20}H_{16}$ clusters allows the formation energy of this interstitial defect to remain relatively low.

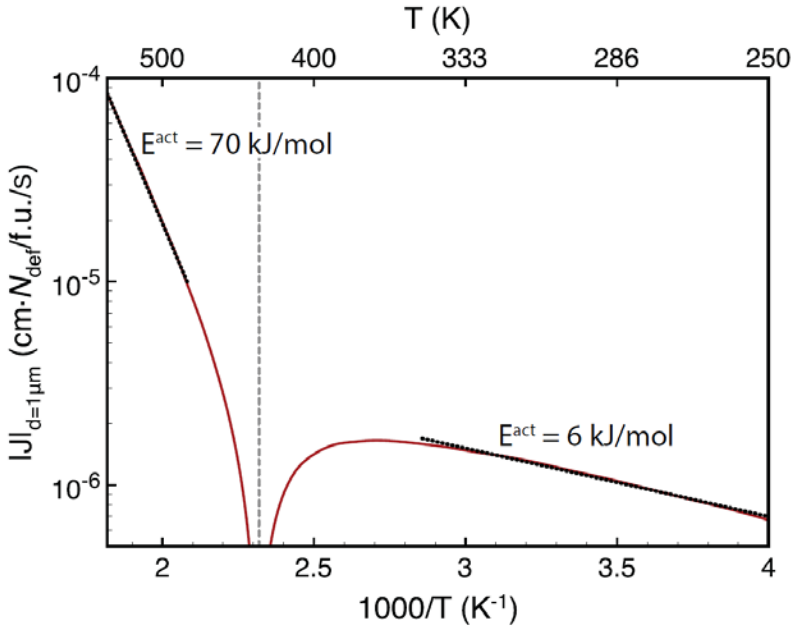

Fig. 3 Calculated flux of interstitial H_2 across a 1 μm region of $B_{20}H_{16}$. The vertical dashed line shows the equilibrium temperature for the reaction. Separate linear fits to high and low temperature regions are shown as dotted black lines along with the associated activation energy.

Having established that interstitial H_2 forms with the lowest energy of all defects, we now turn to the diffusion of this type. From KMC simulations, we find that the energy landscape between interstitial H_2 sites in $B_{20}H_{16}$ is relatively flat and that the largest barrier for diffusion is only 116 meV. Using the concentration gradients obtained from the energies shown in Fig. 2, and the diffusivities obtained from KMC simulations, the overall flux of interstitial H_2 is shown on an Arrhenius plot in Fig. 3. Since the flux depends on the length of the region over which the

concentration gradient is calculated, we have made the arbitrary choice to show the results when the length of the $B_{20}H_{16}$ region is 1 μm; however, such a choice will have no effect on the calculated activation energy since this distance does not depend on temperature. The vertical, dashed line in this figure shows the location of the equilibrium temperature for $B_{20}H_{16} \rightarrow 20B + 8H_2$, where the concentration gradient, and thus flux, decreases to zero since the chemical potential of hydrogen is exactly equal at both interfaces at this temperature. Taking the slopes above and below the critical temperature in Fig. 3, we find that the activation energies for dehydrogenation and rehydrogenation are 70 and 6 kJ/mol respectively. We note that the activation energy, especially for dehydrogenation, is lower than the free energies of formation shown in Fig. 2. Therefore, the mass transport rates in reaction should be sufficiently fast for practical applications. It must be emphasized that rapid mass transport is a necessary, but not sufficient, condition for reaction kinetics that are acceptably fast. Other processes such as nucleation and H_2 dissociation may also limit the reaction rate. However, methods for catalyzing these processes in particular have already been demonstrated in other hydrogen storage systems. With this, the combination of fast mast transport kinetics and large hydrogen content in $B_{20}H_{16}$ makes this material promising for the vehicular storage of hydrogen.

XIV. The synthesis of icosaborane-16 ($B_{20}H_{16}$)

Several methods have been reported for the preparation of icosaborane-16 ($B_{20}H_{16}$) but all were carried out under extreme condition and with as low as 9 to 15% yield. No commercial source is available. The method we plan to use in this project is a modified catalytic pyrolysis of decaborane-14 ($B_{10}H_{14}$). The reported yields for the original procedure are range from 10 to 15 %.

- The synthesis of catalyst, methylaminodimethylborane

A 1:1 molar ratio of methylamine and trimethylborne were condensed in a container and then the mixture was heated 2 hours at 310 □C. The formed products after heated were then opened to traps maintained at -95 °C and -196 °C. The contents of the -95 °C trap were distilled to produce methylaminodimethylborane. The over procedure includes the following two reactions.

$MeNH_2 + BMe_3 \rightarrow MeNH_2BMe_3$ (1)

$MeNH_2BMe_3 \rightarrow MeNHBMe_2 + CH_4$ (2)

- The synthesis of icosaborane-16

Decaborane-14 was charged in a container which is connected a tube. In other container,catalyst of methylaminodimethylborane was charged and also connected to the tube. The flow rate of the both chemicals can be adjusted. Daceborane-14 will be heated at 100 °C and methylaminodimethylborane will kept at 0 °C. Both staring materials are passed through the tube whose middle part will be heated at 350 °C under dynamic vacuum. The other end of the tube connected to pump through a liquid nitrogen trap. The product will deposit just outside the hot zone of the pyrolysis tube. The row product was purified by repeated sublimation.

XV. Characterizing carbon catalysts for mixed $LiBH_4$-$Mg(BH_4)_2$ dehydrogenation/rehydrogenation

We had observed better cyclability in complex metal hydride-carbon composite (~40% metal hydride loading and prepared by room temperature liquid infusion) when the hydride was $LiBH_4$as compared with the mixed $LiBH_4$-$Mg(BH_4)_2$.

Although the mixed hydride $LiBH_4$-$Mg(BH_4)_2$ had better dehydriding property than $LiBH_4$, the poor reversibility is problematic. We set out to determine whether the single hydride, $Mg(BH_4)_2$,

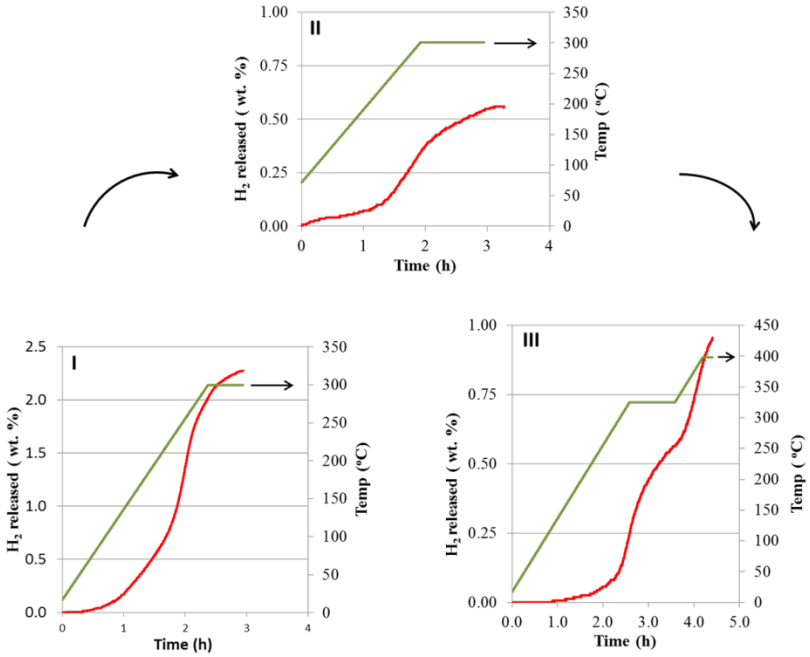

Figure 1 Three dehydriding cycles of $Mg(BH_4)_2$-carbon composite (hydride loading is 34.8 wt.%). After each dehyriding, the sample was rehydrided for 15h at 50 bar H_2 pressure

on carbon can be rehydrided. Figure 1 shows several cycles of hydrogenation and dehydrogenation of $Mg(BH_4)_2$ -carbon composite. H_2 released is expressed as wt. % of the total composite and should be higher if only $Mg(BH_4)_2$was considered. The hydriding was performed at 300 ^oC at 50 bar H_2 pressure for 15 h. The extent of rehydriding was poor compared with $LiBH_4$-carbon composite rehydrided at only 11 bar pressure for 1h and it appeared that the amount of hydrogen released decreased with each cycle. This data seemed in line with literature reports indicating that $Mg(BH_4)_2$ can only be rehydrided under harsh conditions. The proposed cause for the continuous erosion in hydrogen storage property was the formation of $MgB_{12}H_{12}$. Stavilahas reported that $Li_2B_{12}H_{12}$ and $Na_2B_{12}H_{12}$ can be rehydrogenated at conditions that $Ca_2B_{12}H_{12}$ show no rehydrogenation. We propose that the observed difference in the reversibility of composites of carbon-$LiBH_4$ and carbon-$Mg(BH_4)_2$ is due to the difference in the ease of rehydrogenation of the products $Li_2B_{12}H_{12}$ and $MgB_{12}H_{12}$. It has been reported that the H_2 desorption pressure at 300 ^oC in a $LiBH_4$-carbon composite prepared by melt infusion can greatly exceed that dictated by thermodynamics for the decomposition pathway of $LiBH_4$ to LiH+ B +1.5 H_2. However, if a significant fraction of $LiBH_4$ decomposed through the $Li_2B_{12}H_{12}$ ($LiBH_4 \rightarrow 10/12$ LiH + $1/12 Li_2B_{12}H_{12}$ + 13/12 H_2) pathway than higher pressure is possible. The observed pressures from some of our experiments also suggest that a portion of $LiBH_4$ in the composite may decompose through the $Li_2B_{12}H_{12}$ pathway. It is not surprising that in a confined space, clustering of BH_4^- to generate $B_{12}H_{12}^=$ may be facilitated. Thus, the combined facts that decomposition through $Li_2B_{12}H_{12}$ could result in H_2 pressure of practical interest and the fact that rehydrogenation of $Li_2B_{12}H_{12}$ is feasible suggest that the new phase of our research should be

focused on the synthesis of $Li_2B_{12}H_{12}$ and its infusion into carbon to test whether $Li_2B_{12}H_{12}$ is formed in the dehydrogenation and can be rehyrogenated ina $LiBH_4$-carbon composite.

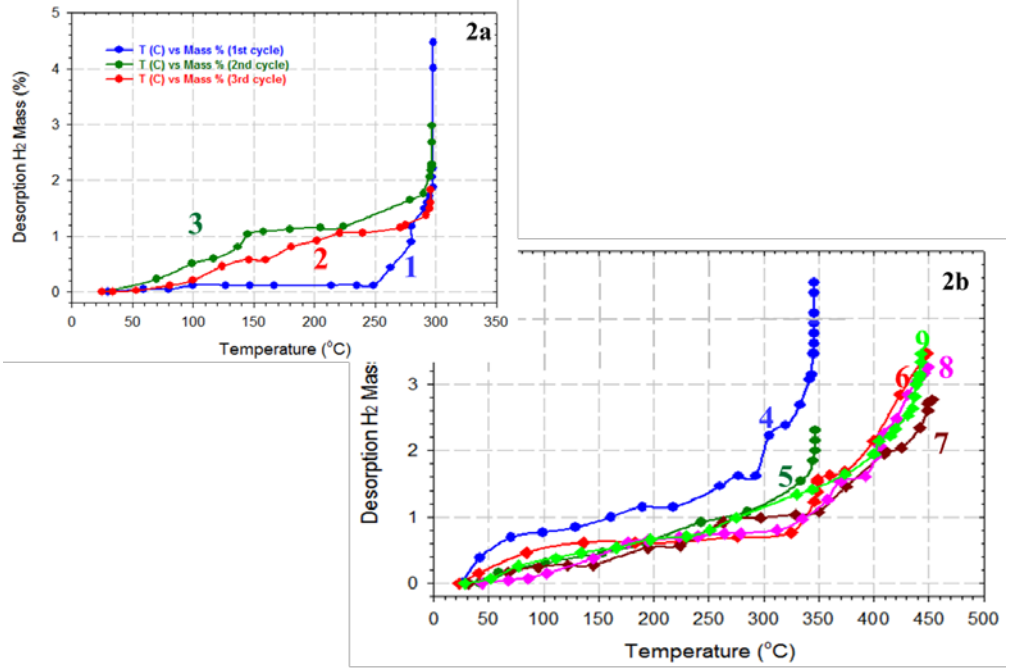

Figure 2a and b H_2 desorption of $LiBH_4$-carbon composite. The numbers indicate the cycle number of desorption. Hydrogenation temperature before desorption was 300 °C for cycles 2-4; 350 °C for cycle 5 and 450 °C for cycles 6-9; pressure was at 2200 psig.

In Fig. 2a, Dehydriding of LiBH4-carbon composite from room temperature to 300°C. (***1***) as prepared composite, (***2***) second cycle of dehydriding after rehydriding at 300°C**,** 2200 psig H_2 pressure, and (***3***) third cycle of dehydriding after rehydriding as in ***2***. The Y axis is with respect to total weight of sample.The lack of low temperature H2 for cycle 1 is possibly because of oxygen and moisture leak into the sample during shipping. Although the increases in H2 pressure in the region below 280 °C were similar for the second and third cycle, there was evidence of some degradation in the storage property with further cycling, as the pressure achieved at 300 °C decreased noticeably in the third cycle. The low temperature features in cycles ***2*** and ***3*** are real because any solvent contaminant would have been pumped away after the first cycle.

After the third cycle at 300 °C, the sample was subjected to two more dehydriding/rehydriding cycles in which the dehydriding was carried out to 350 °C (at the end of this series, the sample would have been subjected to a total of 5 cycles, Fig. 2b) and the rehydriding was also conducted at this temperature. The first dehydriding profile is shown in curve *4* , and it appears to be quite similar to curve *3* of the previous slide. However, the dehydriding profile of the second cycle (curve *5*) indicated further degradation of the H_2 storage property. After this series of experiments, the sample was subjected to four additional cycles of dehydriding/rehydriding with a temperature limit of 450 °C. Within experimental error, all the dehydriding profiles (Figure 2b, curves *6-9*) were the same and similar to curve *5*. Steady and reversible performance has been attained.

Gao et al. proposed that a major reason for the loss in the reversibility in the hydrogen cycle for hydrides confined in carbon nanopores was due to the loss of alkali metals through reactions

with carbon. They observed improved reversibility through the addition of alkali metals to the composite. Our data appears to support their proposal. After the third cycle at 300 °C, the impurities on carbon that could react with the hydride at that temperature was depleted. Therefore, up to300 °C, the dehydriding profile of cycle *4* did not deviate from that of cycle *3* in any significant manner (compare curve *4* and curve *3*). However, cycle *4* terminated at 350 °C, a temperature higher than any of the previous cycles, and as a result further reaction between the hydride and residual carbon impurities took place. This caused additional degradation in the amount of hydrogen released (curve *5*). At this time, all reactive impurities on the carbon were depleted and repeatable dehydriding profiles could be obtained, which were the last four cycles at 450 °C. That reversible behavior can be obtained suggests that, indeed, the physical constraint of the carbon pores can suppress sintering.

XVI. NMR studies of the decomposition products of $2LiBH_4+5Mg(BH_4)_2$

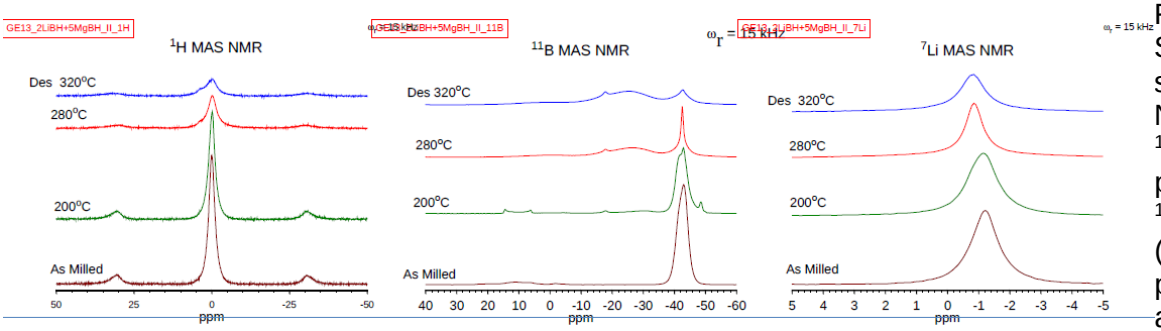

Fig. 1 Solid state NMR ^{1}H (left panel), ^{11}B (middle panel) and ^{7}Li (right panel) spectra upon H2 desorption reactions.

Multinuclear and high resolution (MAS) solid state NMR experiments were performed using a Bruker 500 MHz spectrometer and a Bruker 4mm MAS probe (^{11}B background free): Samples include the as-milled mixture of 2:5 borohydrides and solid residue after H_2 desorption at lower Temperatures. The ex-situ ^{1}H and ^{11}B NMR spectra (Fig. 1) showed eminent decrease of BH_4 (~ -41 ppm peak for both $LiBH_4$ and $Mg(BH_4)_2$) units and their transformation to other boron species. There was no single borane species, B_nH_m, that was identified unambiguously. The borane species was mainly characterized by a broad -26 ppm peak (see next slide) after thermal heating above 280 °C. Note that -26 ppm peak cannot be due to $Li_2B_{12}H_{12}$ of which resonance is expected at -15 ppm.

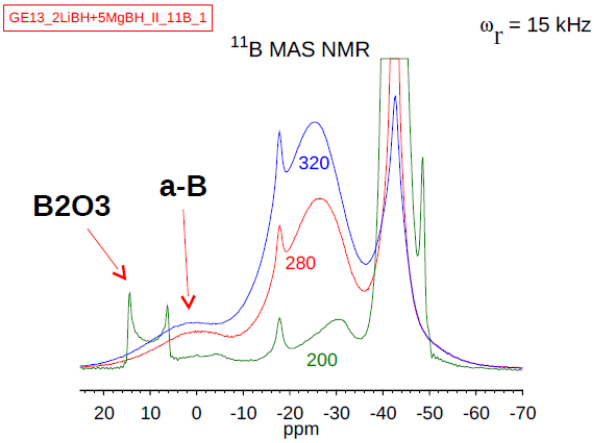

Fig. 2 ^{11}B MAS NMR spectra.

Besides the sharp -17.7 ppm and a broad peak at -1 ppm (amorphous boron), the main -26 ppm peak represents the major boron species. Considering all possible different boron bonding environments1 in B_nH_m, it is quite encouraging to see single resonance to represent the desorption product.

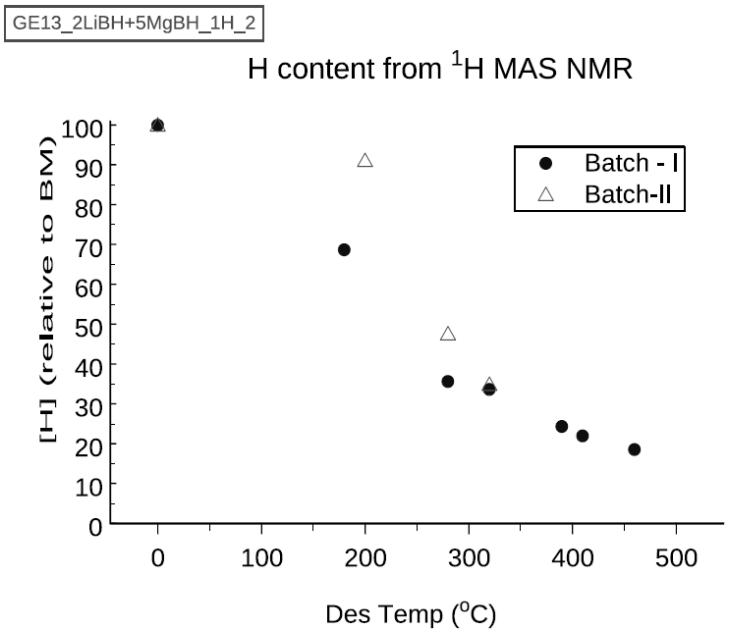

Fig. 3 ^{1}H MAS NMR using two batches.

Before the main -26 ppm peak, a 11B peak at -30.5 ppm appeared upon heating at lower temperature (200 °C). The peak could possibly be assigned to B_3H_8 formation. However, its formation was not in significant quantity, and other sharp peaks at -48.6 ppm and -17.8 ppm were accompanied. After heating at 200 °C, the deduction in hydrogen content measured by 1H NMR was less than 10% (Fig. 3, [H] plot). [H] plot for the new batch showed noticeable difference from the first batch that contains boron oxide in large fraction.

The -48.6 ppm peak might be transient, disappeared at higher temperatures. Such peak at the high field is due to higher B coordination with more 3-center-2 electron bonds around B. Identifying such moiety could be a valuable information in the early stage of dehydrogenation reaction. The -17.7 ppm also formed at low temperature heating, and remained unchanged up to 320 °C. The -17.7 ppm peak can be associated with a stable boron species, such as closoborane: -15.5 ppm for $B_{12}H_{12}$. The -26 ppm cannot be assigned to any of known closo-borane structure although observing the single resonance is highly encouraging.

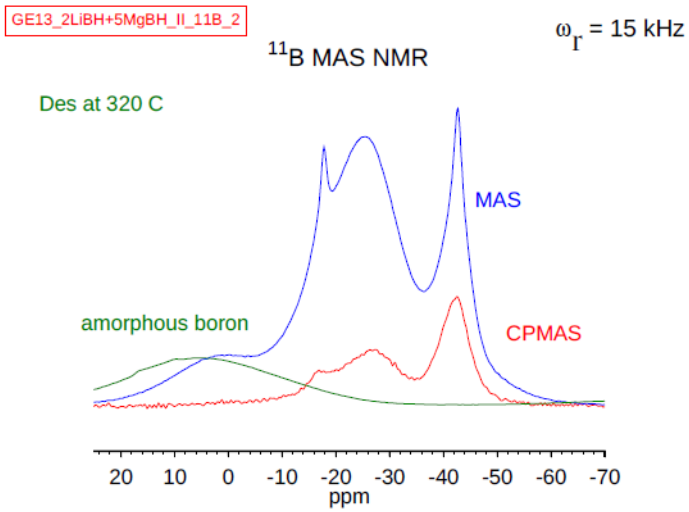

Fig. 4 ^{11}B MAS NMR spectra.

The peak near at 0 ppm is assigned as amorphous boron at the moment. The peak appears at nearly the same position of ^{11}B spectrum of neat amorphous boron (Aldrich). ^{1}H-^{11}B CPMAS (cross-polarization) NMR also supports the nature of the boron species which bears no direct B-H chemical bonds.It is surprising to see the formation of amorphous boron because amorphous boron is not expected from the calculation.

XVII. High-resolution desorption data for the following three prioritized mixtures: $(NH_4)_2(B_{12}H_{12})$, $2LiBH_4 + 5Mg(BH_4)_2$, and $Mg(NH2)_2 + Mg(BH_4)_2$

Our recent experimental efforts focused on obtaining high-resolution desorption and recharging data as well as phase identification for the following three prioritized mixtures: $(NH_4)_2(B_{12}H_{12})$, $2LiBH_4 + 5Mg(BH_4)_2$, and $Mg(NH2)_2 + Mg(BH_4)_2$. Building off of the TPDMS data previously obtained, we focused on phase identification via *in situ* XRD and FTIR experiments as well as WDD to establish reversibility. The XRD measurements were performed in a flowing nitrogen (200 sccm) environment using a sapphire substrate with a temperature ramp of 1° C/min from 50 to 550° C after a 1 hour room-temperature scan. For the variable temperature scans, each scan was integrated for 10 minutes, providing averaged data over a 10° C window. Phases were identified using the MDI JADE software package and the ICDD Powder Diffraction Database. For the FTIR experiments, both diffuse reflectance (DRIFTS) and photo acoustic (PAS) FTIR methods were used. DRIFTS measurements allowed us to explore local environment changes with changes in temperature. The samples to be measured via DRIFTS were contained in a sample holder under flowing argon. The chamber containing the sample holder was purged with nitrogen and the sample temperature ramped at a rate of 5° C/min from room temperature to 450° C. Every minute, 16 sample scans were collected during the temperature ramp and a powdered KBr background was used. For the PAS measurements, the sample holder was purged with helium while the enclosure was purged with nitrogen. All PAS measurements were taken at room temperature, with a carbon black background and collected 32 sample scans for each spectrum. Because of the different WDD conditions used, the details of the measurements are only given in the relevant section below.

1.) **$2LiBH_4 + 5Mg(BH_4)_2$** :The $LiBH_4/Mg(BH_4)_2$ mixture was prepared by ball milling as-purchased $LiBH_4$ and $Mg(BH_4)_2$ in a 2:5 molar ratio. Our XRD measurements [Figure 1] revealed that the mixture resembled a physical mixture of $LiBH_4$ and $Mg(BH_4)_2$, though the peaks corresponding to LiBH4 were partially convoluted with the substrate. The measurements revealed several steps of decomposition: 1) consumption of $LiBH_4$ and partial consumption of $Mg(BH_4)_2$(decreasing intensity of peaks) between 200-250° C. 2) full consumption of $Mg(BH_4)_2$ and possible MgB_2 or MgH_2 formation (250-300°C). 3) Above 350°C, the formation of MgB_2, and the formation of peaks corresponding to an unidentified phase (at 2θ = ~30-40°) .This reaction path differs from that predicted by thermodynamics, which we attribute to kinetic limitations in the system. This conclusion is supported by the difference in observed desorption onset versus the predicted temperature (approximately 200° C vs. -29° C).

   We used WDD to examine the reversibility of this mixture, as well. The experiment was performed by ramping the sample from room temperature to 350° C at 5° C/min and holding for approximately 2 hours. To recharge the system, the temperature was maintained and the sample exposed to 138 bar UHP hydrogen for approximately 18 hours. The process was then repeated for each cycle. We found indications of limited reversibility under the conditions used [Figure 2].

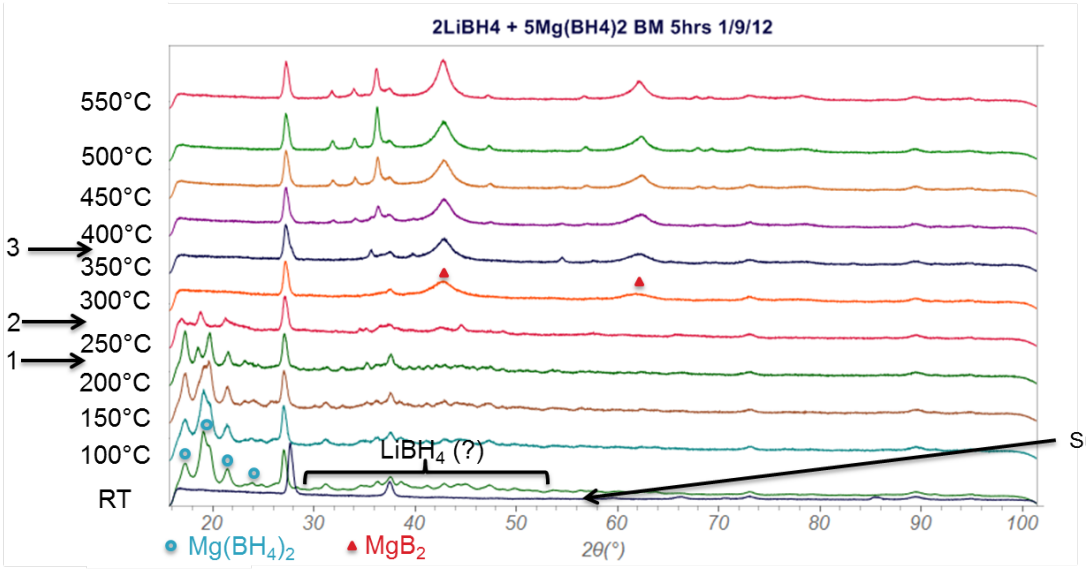

Figure 1. XRD measurements of ball milled $2LiBH_4+5Mg(BH_4)_2$.

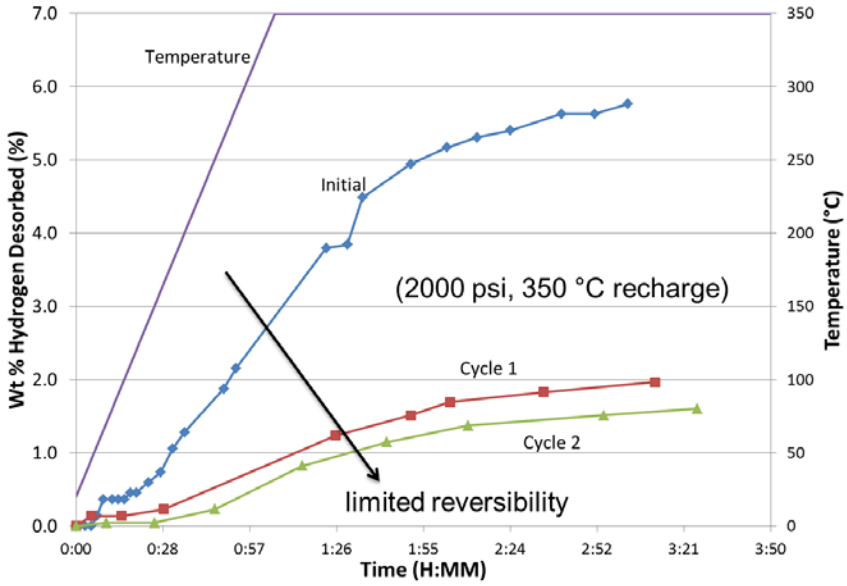

Figure 2. Reversibility studies of mixed $2LiBH_4+5Mg(BH_4)_2$.

2.) **$Mg(NH2)_2$ + $Mg(BH_4)_2$**:The $Mg(NH_2)_2/Mg(BH_4)_2$mixture was produced by ball milling as-purchased $Mg(BH_4)_2$ with $Mg(NH_2)_2$ synthesized from MgH_2 and 20 bar NH_3. Like the $LiBH_4/Mg(BH_4)_2$ mixture, we reported previously that the onset of hydrogen desorption occurs at ~200 °C, a significantly lower temperature than the pristine constituents, with a second hydrogen release event at roughly 400 °. Northwestern and Ford collaborated closely in the identification of the reaction products and pathway, with Ford providing available XRD and IR data to assist in the determination of reaction products via computational methods, including PEGS to determine new structures. However, further study of the system via WDD found it to be irreversible under the conditions tested: 1)

ramp to 250°C at 5°C/min, cool to RT for recharge with 114 bar UHP hydrogen. 2) ramp to 380°C at 5°C/min, maintain for recharge with 138 bar UHP Hydrogen.

3.) **$(NH_4)_2(B_{12}H_{12})$**: This compound was synthesized and kindly provided to Ford by J.C. Zhao (OSU). We reported previously that hydrogen desorption begins at roughly 250 ºC, and occurs in two primary steps. Our TPDMS results indicated that little NH_3 is released and undetectable quantities of diborane or borazine are produced during decomposition. We found evidence of partial reversibility up to 350° C via WDD cycling experiments [Figure 3]. The WDD experiment was carried out as follows:

1. Initial desorption to 250° C at 5° C/min and holding for approximately two hours.
2. Recharge overnight at the above temperature with 138 bar UHP hydrogen.
3. Cool sample to room temperature, purge excess hydrogen from the system.
4. Ramp sample to 250°C at 5°C/min and hold for two hours (Cycle 1, 250° C in [Figure 3].
5. After the two hours at 250° C, the sample was ramped up to 300° Cat 5° C /min and held (Cycle 1, 300° Cin [Figure 3]).
6. Recharge overnight at 300° Cunder 138 bar UHP hydrogen.
7. Repeat process for subsequent temperatures.

XVIII. Screening the Li-Mg-B-N-H system for new hydrogen storage reactions

Metal borohydrides and amides exhibit some of the highest hydrogen capacities among the known solid state materials. Compounds with Li, Mg, B, N, and H are particularly interesting as they involve numerous compounds of potentially high relevance for hydrogen storage:

1) Borohydrides ($LiBH_4$, $MgBH_4$, $Li_2B_{12}H_{12}$, $MgB_{12}H_{12}$)
2) Amides and imides [$LiNH_2$, $Mg(NH_2)_2$, Li_2NH, $MgNH$, $Li_2Mg(NH)_2$, etc.]
3) Borohydride-amide mixed compounds (Li_2BNH_6, $Li_4BN_3H_{10}$)
4) Ammoniated borohydrides [$Mg(BH_4)_2 \bullet 2NH_3$]
5) Ammonia borane and derivatives (BH_3NH_3, BH_2NH_2, $LiBH_2NH_3$, etc.)
6) B-N-H and B-H compounds [B_2H_6, B_4H_{10}, $B_{16}H_{20}$, $B_{20}H_{16}$, $(NH_4)_2B_{12}H_{12}$, etc.]
7) Various reaction products: elements (Li, Mg, B, N_2), metal hydrides (LiH, MgH_2), metal borides (MgB_2, MgB_4, MgB_7), metal nitrides (Mg_2N_3, Li_3N, LiMgN), boro-nitrides (BN, Li_3BN_2, $LiMgBN_2$), etc.

Using density-functional theory (DFT) methods, we have calculated the total crystal binding energies and vibrational free energies of all currently known compounds in the Li-Mg-B-N-H system (approximately 50 compounds). The structures of most of these compounds have been taken from the Inorganic Crystal Structure Database (ICSD). To these, we have added the theoretically predicted compounds whose structures have been obtained using the prototype electrostatic ground state (PEGS) search and other structure prediction methods. The calculated free energies have been used as inputs to the grand-canonical linear programming (GCLP) approach for determining reaction pathways in multinary systems [1]. Using the GCLP method, we have rigorously determined all the thermodynamically allowed reversible reactions in the Li-Mg-B-N-H system which involve the currently known (or predicted) compounds (some of these predictions may change with the discovery of new, currently unknown Li-Mg-B-N-H compounds). Our predictions for the DOE targeted range of temperatures and pressures are given in Table I, and the corresponding van't Hoff plots are shown in Fig. 1.

Reactions	**H_2 wt. %**	**ΔH^{300K} (kJ/mol H_2)**	**ΔS^{300K} (J/mol-K)**
$2(NH_4)_2B_{12}H_{12} \leftrightarrow 4BN + B_{20}H_{16} + 12H_2$	6.81	17	104
$5Mg(BH_4)_2 + 2LiBH_4 \leftrightarrow 5MgH_2 + Li_2B_{12}H_{12} + 13H_2$	8.37	24	104
$6Mg(BH_4)_2 \leftrightarrow 5MgH_2 + MgB_{12}H_{12} + 13H_2$	8.10	29	100
$B_{20}H_{16} \leftrightarrow 20B + 8H_2$	6.95	33	111
$5MgH_2 + MgB_{12}H_{12} \leftrightarrow 6MgB_2 + 11H_2$	7.46	44	115

Table I. Predicted thermodynamically reversible hydrogen storage reactions that fall in (or near) the targeted temperature and pressure window of -40 to 80 ^{o}C and 1 to 700 bar, respectively.

Three of the five reactions in Table I were found by us in an earlier paper [2]. Two of these reactions (#2 and #r in Table I) involve $Mg(BH_4)_2$ and $LiBH_4$ as reactants and $MgB_{12}H_{12}$ and $Li_2B_{12}H_{12}$ as end products. In Ref. [2] we showed that both these reactions possess excellent thermodynamic properties that combine low reaction enthalpies with low entropies. They remain the two most-promising single-step reversible reactions in the Li-Mg-B-N-H system. Finally, a two-step reaction involving ammonium dodekahydro-closo-dodekaborate as the starting material has also been predicted by these calculations:

$$(NH_4)_2B_{12}H_{12} \leftrightarrow 2BN + 0.5B_{20}H_{16} + 6H_2 \leftrightarrow 2BN + 10B + 10H_2.$$

These reactions releases 11.3 wt.% H_2 over both steps. At p=1 bar H_2 pressure, the first step (decomposition of $(NH_4)_2B_{12}H_{12}$ into BN, $B_{20}H_{16}$, and H_2) occurs at -120 ^{o}C, while the second step (decomposition of $B_{20}H_{16}$ into B and H_2) proceeds at 20 ^{o}C. In contrast to the conventional complex hydrides that contain metal cations and complex anions, the above reaction represents a new paradigm where the storage material contains both anionic and cationic complexes.

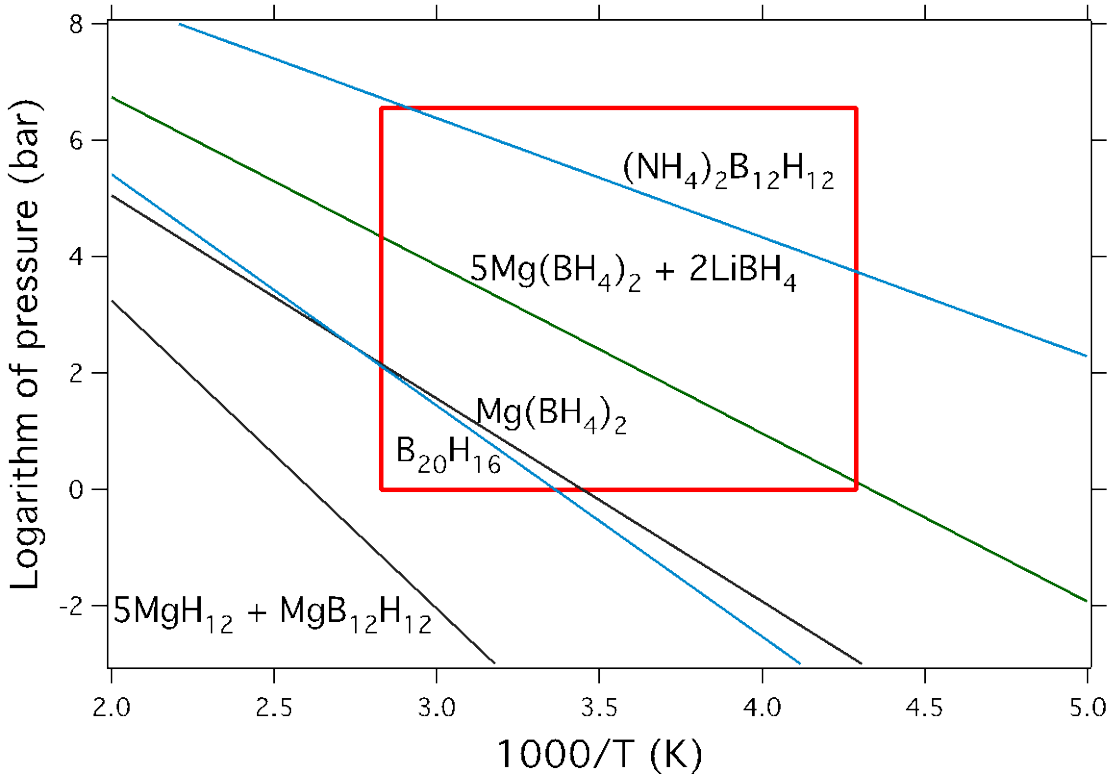

Figure 1. The calculated van't Hoff diagram for the thermodynamically reversible hydrogen storage reactions given in Table I. Each line is labeled by the reactant or the combination of reactants. The red rectangle represents the targeted temperature-pressure window of -40 to 80 ^{o}C and 1 to 700 bar, respectively.

1. Hydrogen storage in the Li-Na-Al-B-H system

The calculations described above have been extended to include alanate-borohydride mixtures. We have calculated the free energies of all known compounds in the Li-Na-Al-B-H system, including metals and metal hydrides (LiH, NaH, AlH_3, $Al_3Na_5H_{14}$), borides (LiB, Li_2B, Li_5B_4, Li_3B_{14}, Li_2B_6, LiB_9, LiB_{11}, Na_2B_{29}, NaB_{15}, Na_3B_{20}, AlB_{10}, AlB_{31}, AlB_{12}, AlB_2, $LiB_{14}Al$, $Na_{0.95}Al_{0.94}B_{14}$), intermetallics (LiAl, Li_3Al_2), boron-hydrogen (B_2H_6, B_6H_{10}, B_5H_9, $B_{20}H_{26}$, $B_{18}H_{22}$, $B_{16}H_{20}$, $B_{13}H_{19}$, $B_{12}H_{16}$, $B_{10}H_{16}$, etc.), metal borohydrides ($LiBH_4$, Li_3BH_6, $Li_2B_{12}H_{12}$, LiBH, $LiBH_2$, $Al(BH_4)_3$, $NaBH_4$, $Na_2B_{12}H_{12}$), and alanates ($LiAlH_4$, Li_3AlH_6, Na_3AlH_6, $NaAlH_4$, $LiNa_2AlH_6$). To these, we have added theoretically predicted mixed alanate-borohydride compounds [e.g., $Li_2AlH_4BH_4$, $Al_3(B_{12}H_{12})_2$] whose structures were obtained using the prototype electrostatic ground state (PEGS) search method. Thermodynamically reversible hydrogen storage reactions were using the grand-canonical linear programming (GCLP) approach. Disappointingly, we did not find any new reactions with favorable thermodynamics in this system.

2. Grand-Canonical Linear Programming (GCLP) method

One of the main shortcomings of the density-functional theory (DFT) studies of complex hydrides is the limited accuracy of the current exchange-correlation functionals, such as those based on the local-density approximation (LDA) or generalized-gradient approximation (GGA). Table I shows that the formation enthalpies of simple hydrides calculated using GGA generally tend to be lower than those measured experimentally by 10-20 kJ/molH_2. Accurate quantum Monte Carlo calculations for MgH_2 have also shown that the GGA errors in the predicted reaction enthalpy for this compound exceed 10 kJ/mol H_2. Similarly, the calculated equilibrium temperature for sodium alanate is found to be underestimated by 70 ^oC, which again can be traced back to GGA errors in the reaction enthalpy. These errors vary in magnitude and therefore cannot be wholly attributed to incorrect GGA total energy for the H_2 molecule. Indeed, in the compounds with metallic bonding (LaH_2, TiH_2, ZrH_2, VH_2) the GGA errors are either small or positive, suggesting that GGA makes errors not only in the H_2 molecule, but also in the bulk compounds, and the magnitude of these errors varies with the type of bonding. This raises concerns that the standard grand-canonical linear programming (GCLP) approach may miss potential reactions due to GGA errors in the relative reaction enthalpies, so that some reactions and/or compounds are incorrectly pushed above the convex hull and therefore missed in GCLP.

We have developed a new, statistically robust version of GCLP, which accounts for the presence of errors in the GGA total energies. The underlying idea is to perturb the set of GGA-calculated free energies by randomly choosing several (typically, between 1 and 3) compounds and adding or subtracting a given amount (typically, 10-20 kJ/mol H_2) to/from the directly calculated GGA free energies. For each set of perturbed free energies, we re-run the GCLP reaction predictions and search for qualitatively different types of reactions appearing on the convex hull. These reactions can then be examined for the likelihood of representing true thermodynamic equilibrium by more accurate quantum mechanical methods, such as Quantum Monte Carlo. Using our GGA results for the Li-Mg-B-N-H system as a test case, we have identified several possible new reactions that could not be found using the standard GCLP approach. It remains an

open question whether these reactions are “real” – which can only be settled by a more accurate calculation or by experiment.

Table I. Comparison of calculated and experimentally measured reaction enthalpies for simple metal hydrides. Experimental values are taken from “Phase diagrams of binary hydrides,” edited by Manchester. Calculations were performed using the Perdew-Wang GGA.

Compound	□H (kJ/mol H_2)		
	T=300 K	Expt.	Error
LiH	169.5	181	-11.5
NaH	93.5	113	-19.5
KH	93.4	115.7	-22.3
RbH	79.7	104.7	-25.0
CsH	82.9	108.1	-25.2
MgH_2	61.1	75.3	-14.2
CaH_2	173.2	181.5	-8.3
SrH_2	169.7	180	-11.3
BaH_2	155.9	177	-21.1
ScH_2	196.2	200	-3.8
YH_2	207.5	218.6	-11.1
LaH_2	191.2	191.2	0
TiH_2	138.3	130.3	+8.0
ZrH_2	157.5	163-166	-7
VH_2	53.5	38.2	+15.3

3. Mass transport and reaction kinetics in borohydrides

a. Lithium borohydride

Borohydrides have high volumetric and gravimetric (18.4 wt. % for $LiBH_4$) hydrogen densities and exhibit partial reversibility, but the kinetics remain very slow at temperatures below their melting point temperatures. Even though the thermodynamic properties of pure $LiBH_4$ are not suitable for on-board storage, we have predicted several destabilized reactions involving $LiBH_4$ with equilibrium reaction temperatures below the melting point of $LiBH_4$. Thermodynamically, these reactions are allowed at temperatures compatible with PEM fuel cells, but almost all of them are inhibited kinetically and require melting of the reactants to show appreciable hydrogen release rates. It is natural to hypothesize that slow rates mass transport in the solid state is a key reason for the slow hydrogen release kinetics in solid. Hence, understanding of the kinetics of solid-state mass transport could provide clues for developing effective catalytic doping strategies.

Thermodynamically, the solid-state dehydrogenation reaction is predicted to occur in the following two-step process:

$$LiBH_4 \rightarrow 1/12\ Li_2B_{12}H_{12} + 5/6\ LiH + 13/12\ H_2 \rightarrow LiH + B + 3/2\ H_2, \quad (1)$$

Our calculation shows that the total reaction enthalpy is □H = 83 kJ/(mol H_2) at T=0 K, in line with the experimentally determined value of □H = 74 kJ/(mol H_2). The calculated enthalpies of the first-step and second-step reactions are 61 and 141 kJ/(mol H_2), respectively.

We have completed a systematic study of mass transport in solid $LiBH_4$ and its decomposition products, $Li_2B_{12}H_{12}$ and LiH, using the theoretical framework that we recently developed to explain the measured activation energies in sodium alanate [Michel & Ozolins 2011; Michel & Ozolins 2014]. This formalism is based on local equilibrium assumptions at interfaces where diffusion is driven by concentration gradients across the phases participating in the reaction. Defect formation energies are calculated from the density-functional theory, and both charged and neutral defects are taken into account. Chemical potentials are set by local equilibrium assumptions at the interfaces (see Figure 2) and lead to nonzero mass fluxes through the participating phases when the temperature deviates from the equilibrium temperature of the reaction. Our results show that defects with the highest concentration in the products LiH and $Li_2B_{12}H_{12}$ are compensating intrinsic defect pairs, the creation of which does not involve exchange of atoms with any of the coexisting phases in the reaction. Hence, their concentration is uniform throughout the sample and they have zero concentration gradients and negligible mass fluxes. In LiH, the dominant defects are Schottky pairs of $[H]^+$ and $[Li]^-$ vacancies, while in $Li_2B_{12}H_{12}$ they are Frenkel pairs of Li^+ interstitials and $[Li]^-$ vacancies. In the reactant $LiBH_4$, negatively charged Li vacancies ($[Li]^-$), positively charged Li interstitials (Li^+), positively charged BH_4 vacancies $[BH_4]^+$, and neutral BH_3 vacancies $[BH_3]$ have the highest concentrations. Among them, only the neutral $[BH_3]$ vacancies have an appreciable concentration gradient, while the others are mutually compensating intrinsic defects with small gradients (see Figure 3).

The structure of the neutral $[BH_3]$ vacancy is shown in Figure 3. It shows that removing a BH3 complex leaves behind a negatively charged H^- anion occupying the vacant site. Compared with the $[AlH_3]$ vacancy diffusion mechanism in NaAlH4 found by Michel & Ozolins (2013), the $[BH_3]$ vacancy diffusion in $LiBH_4$ is blocked by the negative H^- anion left behind after creating the $[BH_3]$ vacancy. The calculated activation energy for moving the H- anion to a neighboring site is approximately 1.6 eV, resulting in the total activation energy of more than 3 eV. We note that due to the high migration barrier of the neutral BH_3 vacancy, the total calculated activation energy is slightly higher as those calculated for the diffusion of charged Li interstitials and vacancies, positively charged BH_4 vacancies, and negatively charged H interstitials. We calculate an activation energy value of 3.1 eV for the diffusion of Li-H interstitial pairs, which is the lowest-energy process found for this system. Hence, we conclude that mass transport in solid $LiBH_4$ is very slow and likely represents a key rate-limiting process of the dehydrogenation reaction based on this material.

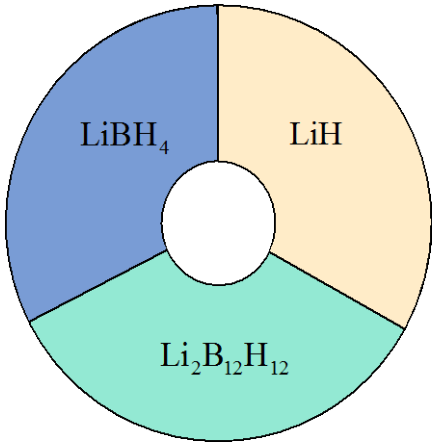

Figure 2. Schematic reaction morphology for reaction (1) showing the possible interfaces, which in turn determine the mass fluxes through the reactant and product phases.

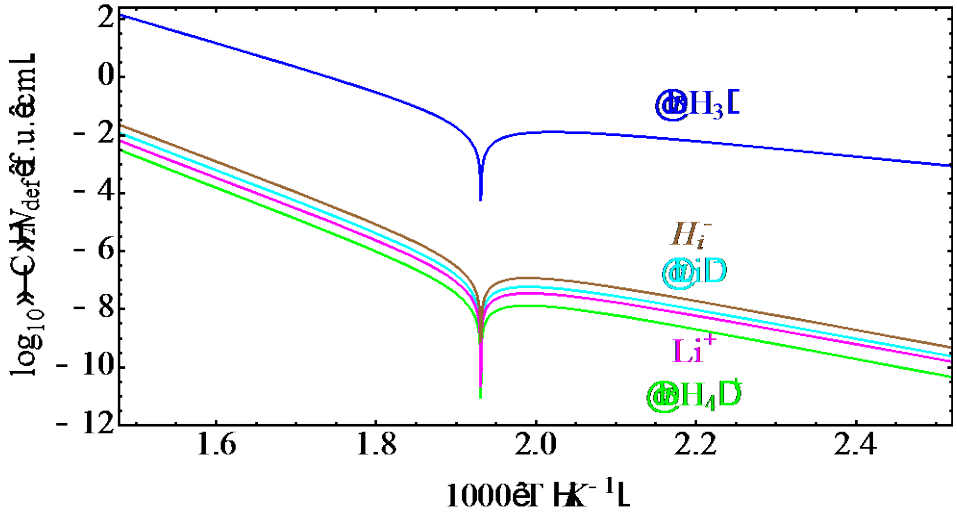

Figure 3. The calculated concentration gradients in $LiBH_4$.

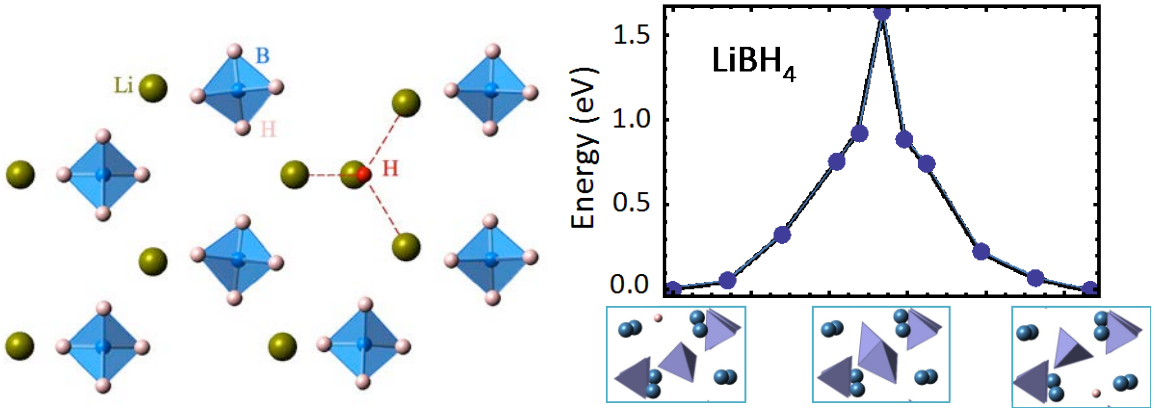

Figure 4. Left: Structure of the neutral [BH_3] vacancy in $LiBH_4$. The H^- anion is shown as red, Li+ cations are dark green, B atoms are blue, and H atoms are pink. Red dashed lines indicate that the H^- anion is tetrahedrally coordinated with the surrounding Li+ cations. Right: Calculated activation barrier for BH3 vacancy diffusion.

b. Magnesium borohydride

Magnesium borohydride, $Mg(BH_4)_2$, has a high volumetric and gravimetric hydrogen density and predicted thermodynamic properties that are almost ideal for reversible on-board hydrogen storage. It can also participate in several destabilized reactions involving $LiBH_4$ with equilibrium reaction temperatures below the 80 ˚C. Finally, partial reversibility has been demonstrated at high temperatures and pressures. Thermodynamically, these reactions are allowed at temperatures compatible with PEM fuel cells, but almost all of them are inhibited kinetically and require melting of the reactants to show appreciable hydrogen release rates. It is natural to hypothesize that slow rates mass transport in the solid state is a key reason for the slow hydrogen release kinetics. Hence, we are have carried out a first-principles study of the kinetics of solid-state mass transport in $Mg(BH_4)_2$. Thermodynamically, the dehydrogenation reaction is predicted to take place as

$$Mg(BH_4)_2 \rightarrow 1/6\ MgB_{12}H_{12} + 5/6\ MgH_2 + 13/6\ H_2.$$

Our calculations show that the total reaction enthalpy is $\Delta H = 40$ kJ/(mol H_2). We have completed a systematic study of mass transport in solid $Mg(BH_4)_2$ and its decomposition products, $MgB_{12}H_{12}$ and MgH_2, using the theoretical framework described in the previous section.

Our results show that neutral BH_3 vacancies in magnesium borohydride ($[BH_3]$) have the highest concentration gradient, while all other concentration gradients are many orders of magnitudes lower (see Figure 5). Removing a neutral BH_3 complex leaves behind a negatively charged H^- anion occupying the vacant site. The preferred diffusion mechanism involves an exchange of a neutral BH_3 complex with a near-neighbor BH_4^- anion as shown in Figure 6. Our DFT results demonstrate that the calculated activation barrier is approximately 2 eV for $Mg(BH_4)_2$ and 1.6 eV for $LiBH_4$; both these values are significantly higher than the calculated migration barrier for AlH_3 vacancies in $NaAlH_4$ (0.34 eV, see Michel & Ozolins, 2011). Together with the significantly lower (by several orders of magnitude) values of the vacancy concentration gradients when compared with those calculated by us for $NaAlH_4$, these results demonstrate that the intrinsic mass transport rates in magnesium borohydride are very slow due to the high energy barrier involved in forming the transition state structure with the doubly negatively charged BH_5 complex. Hence, like in lithium borohydride, the calculated mass transport rates are very slow, suggesting that metal diffusion is a significant and serious bottleneck in hydrogenation kinetics in magnesium borohydride.

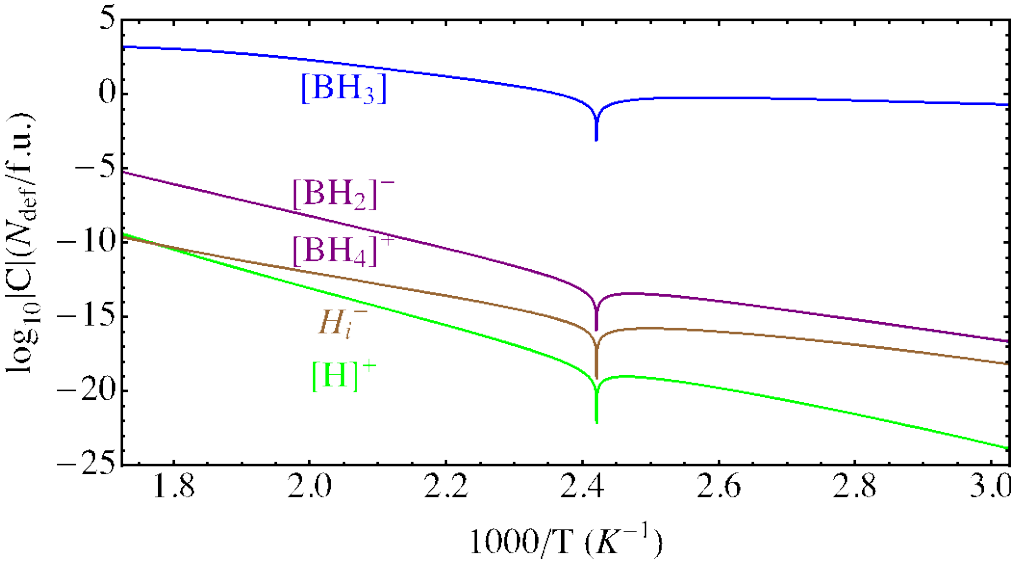

Figure 5. The calculated defect concentrations for native defects in $Mg(BH_4)_2$.

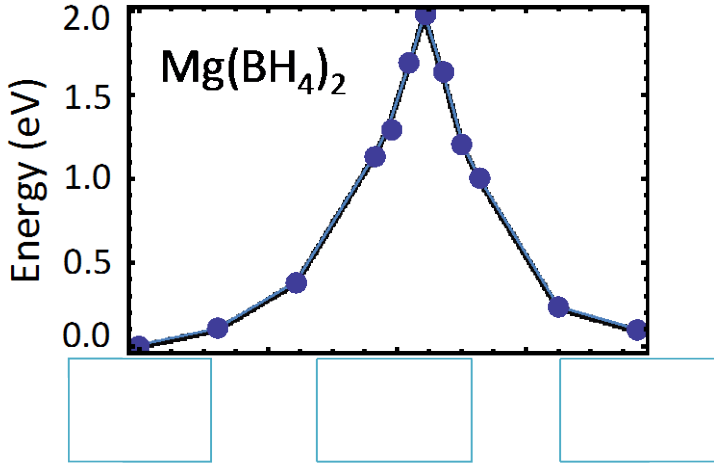

Figure 6. Calculated activation barrier for the diffusion of BH_3 vacancies in $Mg(BH_4)_2$. The H^- anion is colored pink, Mg^{2+} cations are yellow, and BH_n complexes are blue. Left panel shows the initial state with BH_3 vacancy on the lower left, the middle panel is the transition state, and the right panel shows the final state after BH_3 is exchanged between H^- and a neighboring BH_4^-.

REFERENCES

A. Akbarzadeh, V. Ozoliņš, and C. Wolverton, *"First-principles determination of multicomponent hydride phase diagrams: Application to the Li-Mg-N-H system,"* Advanced Materials **19**, 3233-3239 (2007).

V. Ozolins, E. H. Majzoub, and C. Wolverton, *"First-Principles Prediction of Thermodynamically Reversible Hydrogen Storage Reactions in the Li-Mg-Ca-B-H system,"* Journal of the American Chemical Society **131** (1), 230-237 (2009).

K. Michel and V. Ozolins, *"Native defect concentrations in $NaAlH_4$ and Na_3AlH_6,"* Journal of Physical Chemistry C **115**, 21443-21453 (2011). URL: http://dx.doi.org/10.1021/jp203672u.

K. Michel and V. Ozolins, *"Site-substitution of Ti in $NaAlH_4$ and Na_3AlH_6,"* Journal of Physical Chemistry C **115**, 21454-21464 (2011). URL: http://dx.doi.org/10.1021/jp203673s.
K. Michel and V. Ozolins, *"Vacancy diffusion in $NaAlH_4$ and Na_3AlH_6,"* Journal of Physical Chemistry C **115**, 21465-21472 (2011). URL: http://dx.doi.org/10.1021/jp203675e.
K. J. Michel and V. Ozolins, *"Theory of mass transport in sodium alanate,"* Journal of Materials Chemistry A **2** (12), 4438-4448 (2014). URL: http://dx.doi.org/10.1039/C3TA14692H.

XIX. Catalyzing decomposition of complex hydrides

Light complex metal hydrides have excellent gravimetric hydrogen storage capacity, however the kinetics of hydrogen release and uptake are usually too slow for practical applications. The objective of this project is to explore different strategies to accelerate both the dehydrogenation and hydrogenation phases of hydrogen storage. Catalytic decomposition of complex metal hydride is a subject of intense interest but many of the catalysts explored to-date are component specific. For example, although Ti-based catalysts are effective for accelerating $NaALH_4$ dehydrogenation [1], it is ineffective with $Li_3BN_2H_8$ [2]. Thus the first phase of our project was devoted to finding a general catalyst whose reactive mechanism is not metal hydride specific. The second phase of the project was to better integrate this catalyst with the complex metal hydride to further improve the kinetics of hydriding and dehydriding. The third phase was the exploration of the effects of different additives on the dehydriding kinetics.

In the first part of the project, we attempted to find a general catalyst for hydride decomposition and we used $NaAlH_4$ as the test hydride. The approach (Fig.1) was to catalyze hydrogen dissociation using metal nanoparticles supported on carbon and to use carbon as a conduit to move the dissociated hydrogen atoms from the metal to $NaAlH_4$. The experiment was conducted by mixing 70 wt % of $NaAlH_4$ with 30 wt.% activated carbon decorated with metal nanoparticles. Different types of metal nanoparticle-carbon composites were tried and the best catalysts were those based on nickel or cobalt.

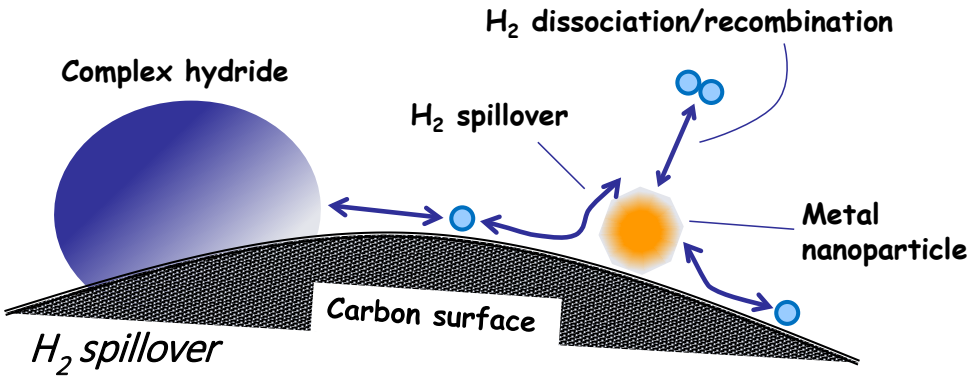

Figure 1 *Strategy for improving the kinetics of dehydriding/hydriding of complex metal hydride*.

The dehydriding kinetics of a physical mixture of 70 wt. % $NaAlH_4$ and 30 wt.% of carbon or carbon decorated with 3 wt.% Co nanoparticles were compared with $NaAlH_4$ alone or $NaAlH_4$ mixed with 5% $TiCl_3$ and the results are depicted in Fig. 2. It was observed that even activated carbon improved the kinetics of dehyriding and further improvement was observed when 3 wt.% cobalt was introduced onto the activated carbon. The dehydrogenation was initiated at a temperature lower than the melting point of bulk $NaAlH_4$, thus, there should not be any melting or infiltration of $NaAlH_4$ into the pores of carbon which could lead to nano-confinement effects. The dehydriding kinetics were still somewhat inferior to the conventional $TiCl_3$ catalyst but further improvement was obtained when both $TiCl_3$ and the carbon decorated with cobalt nanoparticles were mixed with $NaAlH_4$. A dehydrogenated sample of cobalt decorated activated carbon and $NaAlH_4$ could be rehydrogenated up to about 40% at 120 ^oC and 75.8 bar H_2 when no rehydrogenation would take place in the absence of a catalyst.

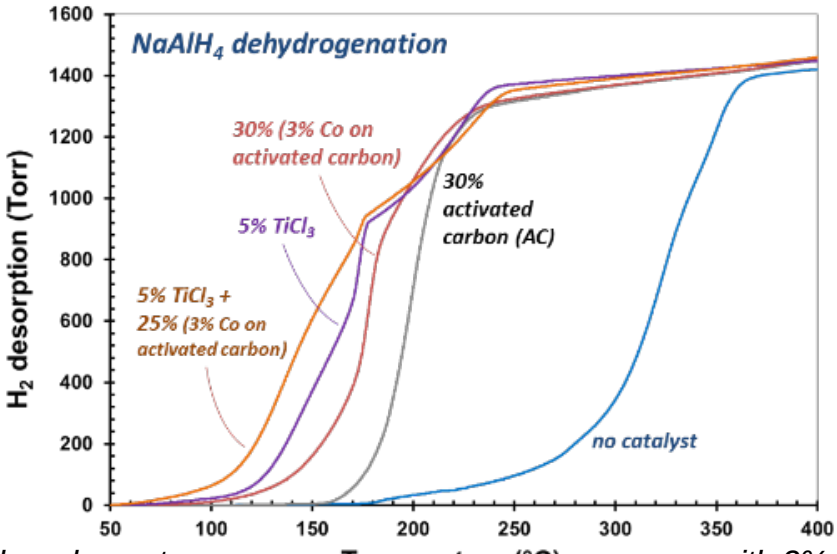

Fig. 2 *Dehydriding profile of $NaAlH_4$, 70% wt.% $NaAlH_4$ and 30wt.% activated carbon, 70 wt.% $NaAlH_4$ and 30 wt.% activated carbon decorate with 3% cobalt, 95 wt. % $NaAlH_4$ and 5% $TiCl_3$, and 70 wt.% $NaAlH_4$ with 5% $TiCl_3$ and 25% cobalt decorated active carbon. The samples were heated at a rate of 5 ^oC/min under 1 bar of H_2.*

The results were encouraging but a physical mixture of cobalt-carbon catalyst and the metal hydride is not the best configuration for utilizing the dissociated hydrogen spilt over from the metal particles onto the carbon. A more intimate mixing of the catalyst and hydride should improve the kinetics as it would increase the contact area between carbon and the hydride. Thus, we investigated the use of low temperature liquid phase infusion technique to prepare a catalyst-hydride composite. This technique differs from the melt infusion technique used to prepare carbon-complex metal hydride composite in the field of hydrogen storage [3]. We proposed that due to the viscosity of the melt, even distribution of the hydride into the small carbon pores may not be optimized. Instead, we utilized low viscosity solution of metal hydride dissolved in THF and multiple impregnation steps of the carbon to improve the distribution of hydride onto the carbon.

We also started to use a carbon molecular sieve with a high surface area of 1800 m^2/g and liquid pore volume of 3.2 ml/g to facilitate the synthesis process. Instead of $NaAlH_4$, we started using $LiBH_4$ as the test hydride because at that time our collaborators in this project had determined a 5:2 mixture of $LiBH_4$ and $Mg(BH_4)_2$ significantly lowered the decomposition temperature of the hydride. We did not use the mixed hydrides initially, as we felt the data from a single metal hydride would be easier to interpret. To facilitate the synthesis procedure, we also switched to use Ni as the hydrogen dissociation/association catalyst on carbon as previously we had discovered that Ni and Co were equally effective in catalyzing $NaAlH_4$ decomposition. The temperature when $LiBH_4$ started to decompose for the $LiBH_4$-Ni-carbon composite was found to be lower than a physical mixture of the hydride and Ni/carbon and more than two hundred degrees lower that of $LiBH_4$ alone. Furthermore, consistent hydrogen evolution profile can be obtained after several cycles of hydriding and dehydriding as is shown in Figures 3A and 3B. We proposed that the partial loss in reversibility observed for the initial cycles was probably due to reaction of $LiBH_4$ with impurities or functional groups on the carbon. After the impurities on the carbon were consumed, the cycling profile became repeatable.

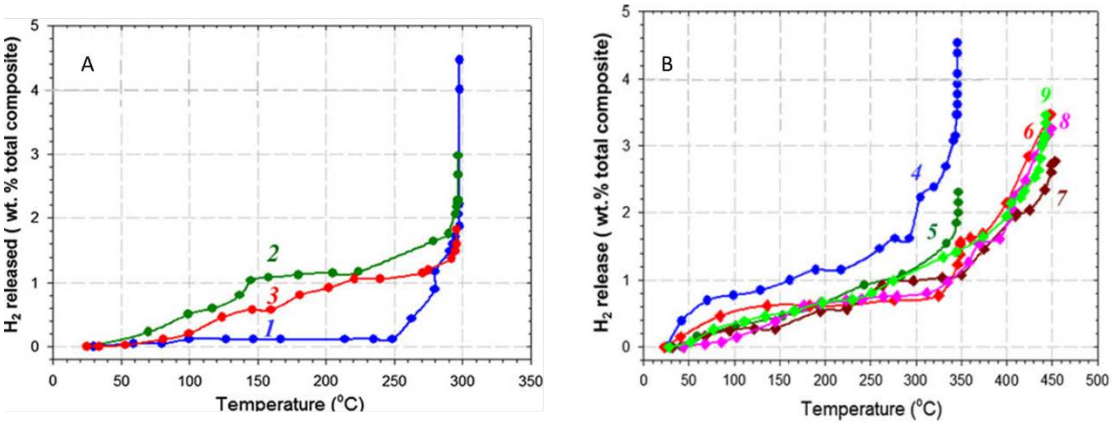

Figure 3 A. *Dehydriding of $LiBH_4$–Ni-carbon composite from 25 °C to 300 °C. (1) as prepared composite, (2) second cycle of dehydriding after rehydriding at 300° C, 2200 psig H_2 pressure, and (3) third cycle of dehydriding after rehydriding as in 2.* **Figure 3B.** *Dehydriding of $LiBH_4$–Ni-carbon composite, used previously in Fig. 3B, from 25 °C to the indicated temperature: (4) first cycle to 350 °C, (5) second cycle to 350 °C, (6) first cycle to 450 °C, (7) second cycle to 450 °C, (8) third cycle to 450 °C, (9) fourth cycle to 450 °C. Before each dehydriding, the samples were hydrided at* 2200 psig H_2, (4) 300 ^{0}C, (5 and 6) 350 ^{0}C, (7–9) 450 °C

After using the infusion technique to prepare $LiBH_4$-Ni-carbon composite, we proceeded to investigate the hydriding and dehydriding profiles of a composite made with $LiBH_4$-$Mg(BH4)_2$-Ni-carbon composite. Although the dehydriding profile was excellent, similar to the observations by our collaborators of the uncatalyzed mixture of the two hydrides, we had difficulties in rehydriding the composite. We attributed the difficulties in rehydriding the mixed hydride composite due to the presence of $Mg(BH_4)_2$. To test this,

we made a composite $Mg(BH_4)_2$-Ni-carbon composite and found that only a small fraction of the composite can be rehydrided.

In the third phase of the project, we studied the effect of other additives to complex metal hydrides that can change the kinetics of dehydrogenation. The most promising additive was $ZnCl_2$. It has been reported that $LiZn_2(BH_4)_5$ completely decomposed at 150 ^oC. The decomposition, however, resulted in the formation of volatile B_2H_6 which essentially rendered this pathway a non-reversible one [4]. We added small amounts of $ZnCl_2$ to a mixture of $Mg(BH_4)_2$ and $LiBH_4$ (molar 0.94:1) and observed enhanced gas evolution at low temperatures and this low temperature gas release was augmented by the addition of carbon (Fig. 4). Analysis of the data using $ZnCl_2$ promotor suggested that the mmoles of gas released at low temperature can be due to formation of $2LiZn_2(BH_4)_5$ which subsequently decomposed to form H_2 as is shown in equation 1. The amount of gas released at low temperature was too much to be accounted for by equation 2, implying that borane formation was not important when small amounts of $ZnCl_2$ was added. The moles of H_2 released per mole of $ZnCl_2$ at low temperature was doubled in the presence of carbon, and this implied that the combination of the two additives can lead to destabilization of the metal hydrides.

$$10LiBH_4 + 4ZnCl_2 = 2LiZn_2(BH_4)_5 + 8LiCl = Zn + \text{Boron byproducts} + 8\,LiCl + 20H_2\uparrow \quad (1)$$

$$10LiBH_4 + 5ZnCl_2 = 5Zn + 10\,LiCl + 5B_2H_6\uparrow + 5H_2\uparrow \quad (2)$$

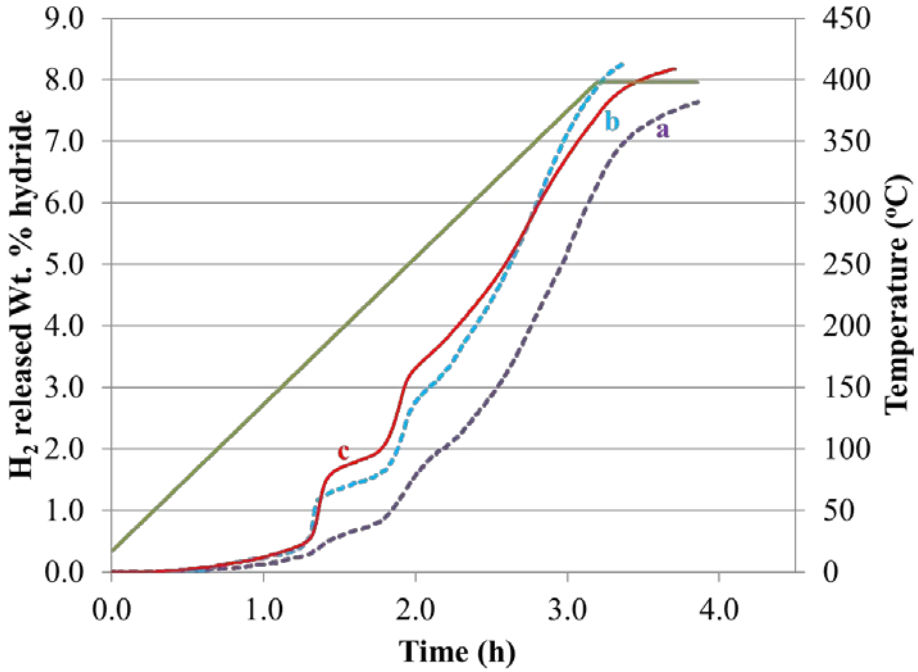

Figure 4 *Effect of $ZnCl_2$ on the dehydrogenation of $Mg(BH_4)_2$ and $LiBH_4$ mixture. (a) hydrides alone; (b) $ZnCl_2$= 21.4 wt.% and (c) $ZnCl_2$+carbon =23.3 wt.% ($ZnCl_2$=17 wt.%). Unlabeled green straight line is the temperature profile.*

In summary, while the research has not achieved the target mandated by DOE, it did find promising lead to follow. In particular, the addition of additives and catalytic material on high surface area carbon seems a promising approach.

References

[1] Bogdanovic B, Schwickardi M (1997) J Alloys Compds 253–254:1–9.
[2] Pinkerton FE, Meyer MS, Meisner GP, Balogh MP (2006) J Phys. Chem B 110:7967–7974.
[3] Liu X, Peaslee D, Jost CZ, Majzoub EH (2010) J Phys Chem C 114:14036–14041.
[4] Ravnsbaek D, Filinchuk Y, Cerenius Y, Jakobsen H J, Besenbacher F, Skibste J, Jensen TR (2009) Angewandte Chemie, International Edition 48 : 6659-6663.

XX. Decomposition of B20H16

In the last quarterly report, we reported on the synthesis and NMR measurements of B20H16 from the laboratory of Prof. Sheldon Shore (deceased). In the past quarter, Prof. Ewan Hamilton of Ohio State provided the small sample (in a sealed bottle) from Prof. Shore's lab to the researchers at Ford, who performed DSC experiments of decomposition. The sample was extremely small; only 1.3 mg of sample could be obtained for the DSC experiment. The conditions for the experiment were: 20 ml/m He flow, heat rate at 5C/m from 20C to 350C, in a Al2O3 crucible. The figure below shows an endothermic peak at about 150 C. We are attempting to scrub more sample out of the bottle for a TPD-MS experiment, but due to the condition and quantity of the sample, the chances are slim. Unfortunately, we have run out of time/funding and also run out of sample, and so we cannot more fully characterize this material and understand the nature of this endothermic peak. Our computational work has predicted a thermodynamic decomposition temperature for B20H16 near room temperature, and it is possible that the peak at 150C represents a (partly kinetically limited) decomposition.

Since we have run out of time and funding, we cannot embark on more synthesis/storage measurements of this compound. However, strongly recommend that DOE continues this work, at least until the material is fully characterized. As we have demonstrated from our computational approaches, there are very few candidate reactions for high-capacity near-ambient reversible storage materials, and of the small number of candidate reactions, all are predicted to have rate-limiting mass transport except B20H16. The combination of 1) high capacity, 2) excellent thermodynamics, and 3) good mass transport kinetics that B20H16 possesses is unique in hydrogen storage reactions, and we recommend that this material be more fully explored.

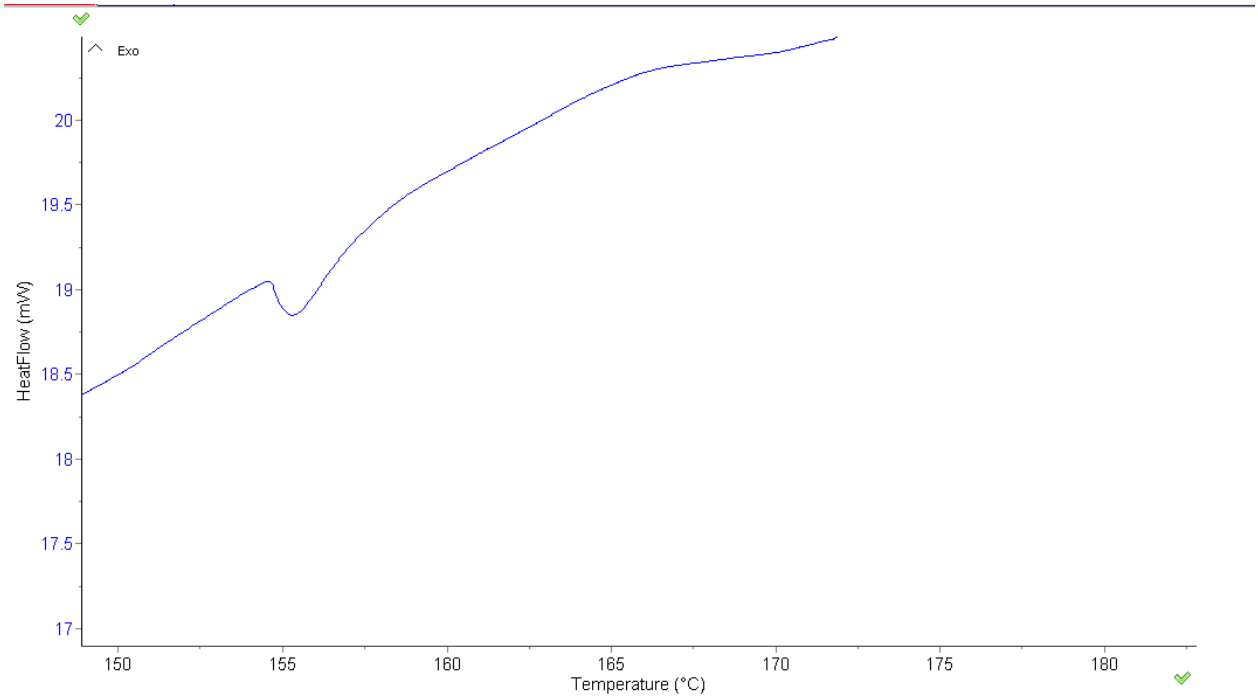

Figure. DSC experiment of B20H16 sample obtained from Prof. Shore's laboratory. The conditions for the experiment were: 20 ml/m He flow, heat rate at 5C/m from 20C to 350C, in a Al2O3 crucible. The data shows an endothermic peak at about 150 C.

Patents: None to report

Presentations (Invited):

C. Wolverton, Gordon Research Conference, “Hydrogen-Metal Systems”, Barga, Italy, July 2013.

Catalytic decomposition of metal hydrides for hydrogen storage application
Sean Lin, Harold Kung and Mayfair Kung
Symposium in Honor of Umit Ozkan: Energy and Fuels Distinguished Researcher

Theoretical prediction of hydrogen storage materials: crystal structures and reaction pathways
Yongsheng Zhang and C. Wolverton
2012 Materials Research Society Spring Meeting, USA, San Francisco, California April 9-13, (2012)

Computational Study of Intermediates and Mass Transport Kinetics in Complex Hydride Reactions
C. Wolverton
International Symposium on Metal-Hydrogen Systems, Kyoto, Japan, Oct. 2012.

Publications

1) Theoretical prediction of different decomposition paths for $Ca(BH_4)_2$ and $Mg(BH_4)_2$
Yongsheng Zhang, Eric Majzoub, Vidvuds Ozolins and C. Wolverton
Phys. Rev. B **82**, 174107 (2010)

2) First-principles prediction of phase stability and crystal structures in Li-Zn and Na-Zn mixed-metal borohydrides
Dilpuneet S. Aidhy and C. Wolverton
Phys. Rev. B **83**, 144111 (2011)

3) Prediction of a $Ca(BH_4)(NH_2)$ quaternary hydrogen storage compound from first-principles calculations
Dilpuneet S. Aidhy, Yongsheng Zhang and C. Wolverton
Phys. Rev. B **84**, 134103 (2011)

4) First-principles prediction of high-capacity, thermodynamically reversible hydrogen storage reactions based on (NH4)2B12H12
W. H. Sun, C. Wolverton, A. R. Akbarzadeh and V. Ozolins
Phys. Rev. B 83, 064112 (2011)

5) Transition Metal-Decorated Activated carbon Catalysts for Dehydrogenation of NaAlH4,
Sean S.-Y. Lin, Jun Yang, and Harold H. Kung,
Int. J. Hydrogen Energy **37**, 2737 (2012)

6) Theoretical prediction of metastable intermediates in the decomposition of $Mg(BH_4)_2$
Yongsheng Zhang, Eric Majzoub, Vidvuds Ozolins and C. Wolverton
J. Phys. Chem. C **116**, 10522 (2012)

7) Crystal structures, phase stabilities, and hydrogen storage properties of metal amidoboranes
Yongsheng Zhang and C. Wolverton
J. Phys. Chem. C **116**, 14224 (2012)

8) First-principles insight into the degeneracy of ground state $LiBH_4$ structures
Yongsheng Zhang, Yongli Wang, Kyle Michel and C. Wolverton
Phys. Rev. B **86**, 094111 (2012)

9) Structure determination of an amorphous compound AlB_4H_{11}
Xuenian Chen, Yongsheng Zhang, Yongli Wang, Wei Zhou, Douglas A. Knight, Teshome B. Yisgedu, Zhenguo Huang, Hima K. Lingam, Beau Billet, Terrence J. Udovic, Terrence J. Udovic, Gibert M. Brown, Sheldon G. Shore, Christopher M. Wolverton and Ji-Cheng Zhao
Chem. Sci. **3**, 3183 (2012)

10) First-principles studies at intermediate products in the decomposition of metal amidoboranes
Yongsheng Zhang, Tom Autrey and C. Wolverton
J. Phys. Chem. C **116**, 26728 (2012)

11) The kinetics of mass transport in $B_{20}H_{16}$
Kyle Michel, Yongsheng Zhang and C. Wolverton
J. Phys. Chem. C **117**, 19295 (2013)

12) First principles studies of phase stability and crystal structures in Li-Zn mixed-metal borohydrides
Yongli Wang, Yongsheng Zhang and C. Wolverton
Phys. Rev. B **88**, 024119 (2013)

13) Hydrogen Storage Properties of Complex Metal Hydride-Carbon Materials
Sean S.-Y. Lin, Jun Yang, Harold H. Kung, Mayfair C. Kung
Topics in Catalysis 56, 1937 (2013).

14) Crystal structure, phase stability, and decomposition of the quaternary Mg-B-N-H hydrogen storage system
Yongsheng Zhang, David Farrell, Jun Yang, Andrea Sudik and C. Wolverton
J. Phys. Chem. C 118, 11193 (2014).

15) Thermodynamic stability of transition metals on the Mg-terminated MgB2 (0001) surface and their effects on hydrogen dissociation and diffusion
Yongli Wang, Kyle Michel, Yongsheng Zhang and C. Wolverton
Phys. Rev. B 91, 155431 (2015).

16) Hydrogen diffusion in MgB_2 bulk
Y.L. Wang, K. Michel, and C. Wolverton
Scripta Materialia **117**, 86 (2016).